Preclinical testing of RRx-001 in mouse models of experimental endometriosis reveals promising therapeutic impacts

Iona McIntyre[1, 2], Vadim Vasilyev[1], Chiara Lia Perrone[1], Priya Dhami[1, 2], Kavita Panir[1, 2], Matthew Rosser[1, 2], Erin Greaves[1, 2]

1. Division of Biomedical Sciences, Warwick Medical School, University of Warwick, Coventry, United Kingdom (UK)
2. Centre for Early Life, University of Warwick, Coventry, UK

Corresponding author: Prof Erin Greaves

Email: Erin.Greaves@Warwick.ac.uk

Tel: 024 7696 8640

Key words: Endometriosis, therapeutic, macrophage

Abstract

Endometriosis is a chronic inflammatory condition characterised by the presence of ectopic endometrial-like tissue (lesions), reduced fertility and chronic pain. Impacting both the health and psycho-social functioning of millions of women worldwide, there is an urgent need for innovative non-hormonal, non-invasive treatments for the disorder. Both peritoneal and lesion-resident macrophages have been strongly implicated in the pathogenesis of endometriosis; key roles include promotion of lesion growth, neuroangiogenesis and nerve sensitization. With such a central role in the disease, macrophages represent a novel therapeutic target. In the current preclinical study, we sought to repurpose the macrophage targeting anti-cancer drug RRx-001 for the treatment of endometriosis. We utilised mouse models of induced endometriosis to demonstrate that RRx-001 induces regression of endometriosis lesions and attenuates pain-like behaviours, without negatively impacting fertility. Targeted depletion of peritoneal cavity macrophages significantly impairs lesion reduction, demonstrating their critical role in mediating the anti-endometriosis impact of RRx-001. Using single nuclei multiomics, we identified a modification of macrophage subpopulations in the peritoneal cavity, specifically reduced acquisition of a pro-disease phenotype and an accumulation of a pro-resolving phenotype. These observations signify the potential of RRx-001 as a novel therapeutic for endometriosis management.

52 **Introduction**

53 Endometriosis is a common, chronic, neuro-inflammatory condition that affects 1 in 10 women (and
54 those assigned female sex at birth) during their reproductive years, although adolescent and
55 postmenopausal cases are well documented(*1*). Endometriosis is defined by ectopic endometrial-like
56 tissue which forms non-neoplastic 'lesions', commonly within the peritoneal cavity and rarely (<1%),
57 in extra-pelvic locations (*2, 3*). Endometriosis has a complex and diverse symptomology which includes
58 severe dysmenorrhea, chronic pelvic pain, dyspareunia, fatigue, and infertility. These symptoms have
59 a cumulative impact on health, well-being, and psychosocial functioning. Beyond the personal impact
60 on those that suffer from the condition and that of their partners and family, endometriosis also
61 represents a substantial socioeconomic burden, due not only to the cost of treatment, but also due to
62 significant reductions in productivity(*4*).

63 Despite the high prevalence of endometriosis, there remains limited etiological understanding
64 of the disease(*5*). Sampsons' theory of retrograde menstruation is the most commonly accepted
65 hypothesis for the origin of endometrial-like tissue within the peritoneal cavity, referring to the reflux
66 of sloughed menstrual debris through the fallopian tubes during menstruation(*6*). Although
67 retrograde menstruation may be common, and reportedly occurring in up to 90% of those with patent
68 fallopian tubes, only a proportion develop endometriosis, indicative of a multifactorial pathogenesis,
69 with immune dysregulation prominent amongst many suspected etiological factors(*7-9*). Following an
70 immunological inability to eliminate refluxed ectopic endometrial fragments, adherence and cell
71 proliferation under hypoxic stress occurs, thus initiating the development of endometriotic lesions(*10,*
72 *11*). The current medical management of endometriosis is non-curative and includes analgesic
73 management, hormonal suppression, and surgical debulking of lesions(*12*). This current strategy is
74 insufficient due to common post-surgical recurrence of lesions, unwanted side-effects from hormonal
75 medications (anovulation and those associated with hypoestrogenism), and a high prevalence of
76 endometriosis-associated pain that is refractory to medical treatment(*13-15*). Thus, there is an urgent,
77 unmet need for novel non-hormonal therapeutics for endometriosis.

78 Macrophages have been strongly implicated in the promotion of endometriosis, emerging as
79 a potential target for a non-hormonal endometriosis therapy(*16*). These dynamic mononuclear
80 phagocytes are present in all tissues, playing integral roles in innate immunity, tissue homeostasis,
81 and the induction and resolution of sterile inflammation. Macrophages demonstrate considerable
82 transcriptional and phenotypical plasticity, existing on a broad spectrum between two highly polarised
83 states: pro-inflammatory and pro-repair, with a varied and dynamic functionality(*17*). Macrophage
84 function is dependent on both the perception of extracellular signals within the tissue niche and

85 cellular ontogeny: seeded pre-birth from the embryonic yolk sac/fetal liver, or monocyte-derived and
86 recruited from the circulation(*18, 19*).
87 In endometriosis, macrophages (and their precursors, monocytes) are an important
88 component of the intra- and extra-lesion microenvironment. They are continuously recruited and play
89 pathophysiological roles in lesion establishment, angiogenesis, and nociception(*20, 21*). In both
90 patients and animal models, pro-endometriosis macrophages have been demonstrated to trend
91 predominantly towards a pro-repair phenotype(*22, 23*). However, broad heterogeneity in peritoneal
92 and lesion-resident populations has been revealed in detailed analyses using techniques such as single
93 cell RNA-sequencing (scRNA-seq) and mass cytometry by time-of-flight (mass CyTOF), demonstrating
94 subpopulations across the spectrum, playing subtype-specific roles in the progression or regression of
95 endometriosis(*24-27*). An inability of macrophages to sufficiently recognise and clear refluxed ectopic
96 endometrial-like tissue, alongside deficient phagocytic capabilities, have been identified in several
97 studies(*28*). In the peritoneal cavity of mice, the predominant macrophage populations are small
98 peritoneal macrophages (SpM) and large peritoneal macrophages (LpM), with monocyte-derived LpM
99 demonstrated to be protective against endometriosis development, possibly due to enhanced lipid
100 metabolism and cholesterol efflux, highlighting an intrinsic link between macrophage ontogeny and
101 functionality(*26, 29*). Conversely, endometrial-derived lesion-resident macrophages enhance lesion
102 growth(*26, 29*) and monocytes that are recruited directly to lesions from the vasculature differentiate
103 *in situ* into macrophages that exhibit a pro-disease phenotype(*26*). Macrophages and monocyte
104 subpopulations are also altered in the endometrium and peripheral blood of women with
105 endometriosis, suggesting systemic myeloid dysfunction(*30*).
106
107 Parallels in phenotype and function can be drawn between macrophages in endometriosis and solid
108 cancers. As with lesions, monocytes are continuously recruited into tumour tissues where they
109 differentiate into macrophages. Niche specific factors, including hypoxic stress, lead to phenotype
110 specification and pro-disease functions and an attenuation of phagocytic capabilities(*31*). Tumour
111 associated macrophages (TAM) are broadly described as having a pro-repair phenotype, however,
112 similar to endometriosis macrophages, deep immunophenotyping has identified diverse TAM
113 subpopulations across the phenotypic continuum, including macrophages in highly phagocytic,
114 cytotoxic, and potentially anti-tumorigenic states(*32-34*). Paradoxically, when appropriately polarised,
115 tumour-resident macrophages can mediate cancer cell phagocytosis, and enhance tumour
116 clearance(*35*). Multiple anti-cancer immunotherapies that reprogram TAMs have emerged in recent
117 years, aiming to alter pro-tumorigenic phenotypes and enhance tumour-clearing activity(*36*). Due to
118 the inherent similarities between the immunopathophysiology, and recent single cell analysis

119 revealing the presence of pro-disease TAM-like macrophages within endometriotic lesions(*26*), we
120 have sought to repurpose the therapeutic strategy of macrophage repolarisation for endometriosis.
121 RRx-001 is a first-in-class small molecule inhibitor currently in several phase I-III clinical trials
122 for a variety of solid cancers, with properties linked to multiple mechanisms of activity including
123 macrophage modulation, phagocytic enhancement, vascular normalisation, inflammasome inhibition
124 and epigenetic modifications, amongst others(*37*). In the current study, we have evaluated the impact
125 of RRx-001 in preclinical mouse models of experimental endometriosis to determine the effect on
126 endometriotic lesion growth and associated pain-like behaviours, and to identify any impacts on
127 oestrous cyclicity and reproductive outcomes. As RRx-001 is known to modulate macrophage
128 phenotype, we investigated the impact of targeted peritoneal cavity macrophage depletion and
129 utilised 10x multiomic sequencing to investigate the transcriptomic and epigenetic landscape of
130 peritoneal macrophages isolated from mice with induced endometriosis, dosed with or without RRx-
131 001. Collectively, we describe vital preclinical data that indicates RRx-001 could be a promising new
132 therapeutic for endometriosis
133
134 **Results**
135 **RRx-001 reduced endometriotic lesion growth and attenuated pain-like behaviours in a 'menses'**
136 **mouse model of experimental endometriosis**. Initially, we assessed the therapeutic potential of RRx-
137 001 for endometriosis treatment, utilising a pre-treatment approach in a syngeneic bioluminescent
138 'menses' mouse model of induced endometriosis. As macrophages are essential in the early
139 establishment of lesions, a pre-treatment approach was used to evaluate whether RRx-001 altered
140 lesion initiation or subsequent progression. In brief, ovariectomised recipient mice received an
141 intraperitoneal injection of 'menses'-like endometrium and oestradiol supplementation(*38*). Mice
142 were randomly assigned to a treatment group and received either intravenous injection of RRx-001 or
143 vehicle control, 6 hours prior to donor tissue transfer, and then twice weekly for 2 weeks (Fig.1A). *In*
144 *vivo* bioluminescent imaging at days 3, 7, 10 and 14 was performed for continuous monitoring of
145 lesions. In both the vehicle control and RRx-001 treated groups, lesions were detectable from day 3
146 onwards, demonstrating that RRx-001 does not prevent initial lesion development (Figs. 1B, 1C). Some
147 spontaneous resolution and/or lesion progression was observed in the 'menses' model of
148 endometriosis (as previously documented(*39*)), leading to high intragroup variability of
149 bioluminescent signal(*38*). Despite the occurrence of some spontaneous resolution, there was no
150 significant difference in bioluminescent signal across the vehicle group at different timepoints.
151 Conversely, mice dosed with RRx-001 exhibited a reduction between days 3 and 7, and days 3 and 14
152 ($p=0.0079$ and $p=0.020$, respectively; Fig.1C). Lesions were recovered at day 14 and histologically

153 verified (Fig.S1); mice dosed with RRx-001 exhibited decreased lesion number (p=0.013; Fig.1D) and a
154 reduced cross-sectional lesion area (median = 1.48 mm^2), compared to vehicle control (median = 4
155 mm^2, p=0.04; Fig.1E). To determine if RRx-001 attenuated evoked pain-like behaviours, mechanical
156 hyperalgesia was assessed using von Frey filaments on days 11, 12 and 13 post-lesion induction. Mice
157 that received RRx-001 exhibited an increased abdominal retraction threshold (p=0.0004; Fig.1F),
158 implying reduced abdominal sensitivity, possibly due to the resolution of lesions within the peritoneal
159 cavity. No differences were observed in hind paw withdrawal measurements (Fig.1G).
160 We performed flow cytometry analysis on the peritoneal lavage of endometriosis mice
161 treated with or without RRx-001 and found no alteration in the abundance of LpM or SpM populations
162 (Fig.S2A and C-D, gating strategy in Fig.S2F). As RRx-001 has been reported to modulate macrophage
163 phenotype, and was previously found to attenuate expression of Sirpα(*40*) (receptor Sirpα-Cd47
164 ligand interaction protects 'self' cells from phagocytosis), we investigated the expression of Sirpα on
165 peritoneal macrophages; expression was increased on LpM isolated from mice with induced
166 endometriosis when compared with naïve mice (no procedures) (p = 0.0046, Fig.S2B and E) and RRx-
167 001 treatment attenuated Sirpα levels (p=0.0053; Fig.S1H).
168
169 **Depletion of macrophages by clodronate compromises the efficacy of RRx-001.** As our initial findings
170 indicated that treatment with RRx-001 led to lesion clearance and phenotypical modulation of
171 peritoneal macrophages, but did not prevent lesion establishment, we next assessed the therapeutic
172 impact of RRx-001 in a model of established endometriotic lesions with concomitant macrophage
173 depletion, to confirm that the anti-endometriosis impact seen was driven by macrophages, as
174 previously described in anticancer studies *(58)*. Mice were randomly assigned to a treatment group
175 (I) RRx-001 or (II) RRx-001+clodronate and then received an injection of 'menses-like' endometrium.
176 Following a one-week period of lesion establishment, mice received 3 intravenous doses of RRx-001,
177 alongside intraperitoneal liposomal clodronate for targeted macrophage depletion in the RRx-
178 001+clodronate group (Fig.2A). Depletion of peritoneal macrophages in the RRx-001+clodronate
179 group was confirmed using flow cytometry analysis, with the proportion of peritoneal macrophages
180 significantly reduced compared to the RRx-001 group (p= 0.0286, Figs.2B, 2C). *In vivo* bioluminescent
181 imaging was performed at day 7 (pre-treatment) and day 14 (post-treatment) (Fig.2D). No difference
182 in lesion bioluminescence was detected between groups at day 7 (Fig.2E). At day 14, following
183 treatment, a significant difference in lesion bioluminescence was observed between treatment groups
184 (p=0.0173, Fig.2E), with mice treated with RRx-001 alone exhibiting reduced lesion bioluminescence,
185 and the RRx-001+clodronate mice exhibiting increased lesion bioluminescence, suggesting a critical
186 role for macrophages in mediating the therapeutic effect of RRx-001 .

187

188 **RRx-001 reduced endometriotic lesion growth and attenuated evoked *and* non-evoked pain-like**
189 **behaviours in a minimally invasive mouse model of experimental endometriosis.** To extend our pre-
190 clinical testing of RRx-001, we utilised an additional, complementary mouse model of endometriosis.
191 In this minimally invasive bioluminescent model, full thickness uterine fragments were injected
192 intraperitoneally into intact recipient mice. Lesions established in this model exhibit less spontaneous
193 regression and improved longevity(*38*), and since recipients are intact, post-incision pain sensitivity is
194 avoided allowing improved pain behaviour testing (*41, 42*). Mice received a full thickness tissue
195 transfer (day 0); one week following lesion induction, mice were dosed (day 8) with either RRx-001 or
196 vehicle, according to randomly assigned treatment groups, and then twice weekly for 2 weeks (Fig.2F).
197 Mice exposed to RRx-001 exhibited a reduction in lesion bioluminescence at day 21 compared to day
198 7 (pre-treatment) (p=0.25; Figs.2G, 2H). No reduction in bioluminescence was observed in the vehicle
199 group. Lesions were recovered at day 21 and histologically verified. The RRx-001 group fewer lesions
200 (p=0.0056; Fig.2I) and a reduced cross-sectional area (median = 1.6 mm^2) compared to the vehicle
201 treated mice (median = 3.1 mm^2, p=0.020; Fig.2J).

202 To perform a comprehensive investigation into the impact of RRx-001 on endometriosis-
203 associated pain, we used multiple evoked and non-evoked behavioural tests at i) baseline (pre-
204 endometriosis induction), ii) after endometriosis induction but prior to treatment (days 7/8) and iii)
205 after RRx-001/vehicle treatment (days 17/18; Fig.2A). To determine if RRx-001 treatment led to an
206 attenuation of evoked pain-like behaviours, mechanical and thermal allodynia were assessed using
207 von Frey filaments and the hot plate test, respectively. We did not detect any significant differences
208 between groups prior to endometriosis induction (day -1/-2) or pre-treatment (day 7/8) across evoked
209 behavioural tests (Fig.3A-C). Post treatment, RRx-001 treatment led to a significant decrease in
210 mechanical allodynia, with increased withdrawal thresholds in both abdominal (p=0.002; Fig.3A) and
211 hind paw measurements (p=0.013; Fig.3B). A significant increase in hot plate latency at day 17 in RRx-
212 001 treated mice (p=0.0064; Fig.3C) was also detected. Next, we assessed the impact of RRx-001 on
213 non-evoked pain-like behaviour using thermal plate preference and the ethologically relevant
214 measures, burrowing and nesting. Burrowing and nesting are known to be reduced or eliminated with
215 decreased well-being and can therefore be used as a surrogate marker of visceral pain evoked by
216 endometriosis(*43*). Prior to endometriosis induction or pre-treatment at days 7/8, we did not detect
217 any statistical differences between RRx-001 and vehicle groups in non-evoked behavioural tests
218 (Fig.3D-F). Post treatment, thermal plate preference testing (TPPT) revealed a significant difference
219 between groups at day 18 (p=0.005; Fig.3D) which may be indicative of a potential alleviation of
220 hypothermal sensitivities following RRx-001 treatment. Of note, mice exhibited only exploratory

221 behaviour on the cold plate, whereas the warm plate was also used for grooming by all mice,
222 suggesting a thermal preference for warmth, as opposed to cold allodynia. No post-treatment
223 differences were identified in burrowing behaviour between experimental groups (Fig.3E). RRx-001
224 treated mice did exhibit significantly increased nest complexity score ($p<0.0001$, Fig.3F, representative
225 nest images shown in Fig.3G) indicating improved well-being due to an attenuation of endometriosis-
226 associated pain.
227
228 **RRx-001 impacts the transcriptomic and epigenomic landscape of peritoneal macrophages in mice**
229 **with induced endometriosis.** 10x single nuclei multiomic profiling was used to generate paired RNA
230 and ATAC libraries for sequencing to investigate the transcriptomic and epigenomic impacts of RRx-
231 001 on peritoneal macrophages (Fig.4A). For this experiment, we used the 'menses' model of induced
232 endometriosis, as the intraperitoneal injection of decidualised endometrial tissue most closely
233 recapitulates the refluxed menstrual tissue thought to initiate endometriotic lesions. At day 7 post-
234 lesion induction, fluorescent activated cell sorting (FACs) was utilised to isolate lineage-, Cd45+
235 leukocytes from the peritoneal lavage of RRx-001 and vehicle treated endometriosis mice, as well as
236 sham controls (n=9, n=5, n=3, respectively, Fig.S3A), followed by multiomic processing using the 10X
237 pipeline. We performed an integrative analysis of peritoneal macrophages combining both modalities
238 into a 'weighted-nearest-neighbour' (WNN) framework, with any cells identified as non-macrophages
239 removed (Fig.S3B-E)(*44*). UMAP projection revealed 7 macrophage clusters; inset shows the samples
240 split by library ID (Fig.4B). We found consistent weighting of RNA and ATAC across clusters (although
241 an increased RNA modality weight was seen in the proliferative cluster), uniformity of high-quality
242 nucleosome signal (ATAC) and a consistently high log10GenesPerUMI (RNA) (Fig.S3C). All peritoneal
243 macrophage clusters were *Cd45*+ and *Cd11b*+, and feature plots of *H2-Ab1* and *Adgre1* enable
244 visualisation of SpM by low *Adgre1* (F4/80) and high *H2-Ab1* (MHCII) expression, prototypical LpM
245 with high *Adgre1* and low *H2-Ab1*, and intermediate *Adgre1* in other LpM populations, as previously
246 characterised in mice with induced endometriosis at the single cell level(*26, 45*) (Fig.4C).
247 An analysis of sample composition by cluster revealed macrophage subpopulations were
248 shared between experimental groups. Prototypical LpM (defined by *Timd4* and characteristic DEGs
249 *Prg4*, *Ltbp1*, *Alox15*) exhibited comparable proportions in each sample, as did proliferative LpM and
250 SpM. The predominant population in the vehicle treated endometriosis mice, termed pro-disease
251 LpM, expressed the DEGs *F13a1, Gas6, Lyve1* and *Nrp1*, previously linked to endometriosis(*30, 45*),
252 this population was markedly reduced in both RRx-001 treated and sham mice (Fig.4D,E). In RRx-001
253 treated mice, the predominant population was termed pro-resolving LpM due to the associated lesion
254 resolution observed and the expression of genes such as *Ms4a4*, *Ccr2*, *Calhm6*, *Fcrla* and *Saa3*

255 associated with inflammatory monocyte-derived infiltration, response to pathogens / antigens and
256 lipid-associated phenotypes, previously linked to lesion resolution (Fig.4D,E)(*26, 29*). We included
257 sham mice in this analysis, which exhibit a post-surgical loss and subsequent replenishment of
258 prototypical LpM and therefore model a resolution of transient inflammation. As expected, transitory
259 LpM were predominant in sham mice; both populations expressed intermediate levels of *Adgre1* and
260 *Timd4* and were separated by enhanced *Vsig4* expression (in transitory LpM 1; Fig.4D,E), a gene known
261 to represent longer time-in-residency, suggesting transitory LpM1 have been present in the peritoneal
262 niche longer than transitory LpM2(*46*).

263 Abundant expression of *Ccr2* and low *Timd4* on SpM and pro-resolving LpM indicated recent
264 recruitment/monocytic-derivation of these populations, an ontogeny previously shown to be
265 protective against endometriosis development(*29*); paired ATAC data also demonstrated increased
266 chromatin accessibility of the *Ccr2* gene in these populations and significant peak-gene links (Fig.4F).
267 Top DEGs separating pro-resolving and pro-disease LpM were those linked with monocytic ontogeny
268 and complement protein C1q as well as *Saa3* (Fig.4G). Enhanced mRNA levels of the transcription
269 factor, *Cebpb* (associated with regulating macrophage lipid metabolism and phagocytosis(*47*)) were
270 evident in the pro-resolving population (Fig.4G), suggesting enhanced Cebpb regulation of this
271 phenotype. Conversely, transcription factor footprinting did not support this; with comparable
272 enrichment observed in pro-resolving, pro-disease and prototypical populations. Expected
273 footprinting differences, such as the characteristic Gata6 control of prototypical LpM, were detectable
274 in the ATAC data, with most enrichment observed in prototypical LpM and least enrichment observed
275 in pro-disease LpM (Fig.4H)(*48*). We also performed DNA sequence motif enrichment analysis of the
276 ATAC data to identify overrepresented motifs in the differentially accessible peaks of RRx-001 treated
277 mice (all macrophages), with hypergeometric probability testing of enrichment against a set of
278 background peaks matched for GC content. We identified a strong enrichment of Kruppel-like factor
279 motifs (Klf15, Klf14, Klf2), with Klf family members having broadly reported roles in the activation and
280 polarisation of macrophages, recent research has identified highly specific and unexpected roles in
281 macrophage differentiation for these broadly expressed transcription factors(*49*). The greatest
282 overrepresentation was seen in the Klf14 (4.03-fold enriched, $p < 0.0001$) and Klf15 (2.91-fold
283 enriched, $p < 0.0001$) motifs, which alongside Klf2, have been linked to modulation of inflammatory
284 signalling pathways. Sp4 and 9 motifs were also enriched (3.06-fold and 2.96-fold enrichment
285 respectively). Of particular interest was the enrichment of Nrf1 motifs (5.29-fold enrichment,
286 $p<0.0001$); RRx-001 has previously been shown to induce Nrf2 which mediates an antioxidant
287 response(*50*). Nrf1 works in concert with other transcription factors such as Nrf2 to modulate cellular
288 responses to oxidative stress and maintain cellular homeostasis.

289 Next, slingshot was used to perform cell lineage and pseudotime inference analysis on
290 reduced dimensional data using previously identified WNN clusters. SpM was specified as the initial
291 cluster as the infiltration and transformation of monocytes into SpM with eventual differentiation into
292 LpM is known to occur under inflammatory conditions, such as endometriosis. Lineage inference
293 identified three branching trajectories from SpM (Fig.5A)(*23*); pseudo-temporal trajectories to the
294 terminal populations of pro-disease LpM, prototypical LpM and proliferative LpM were identified.
295 Interestingly, pro-resolving LpM appeared to be an intermediate in all trajectories, further supportive
296 of a recent monocyte-derived ontogeny for this population (Fig.5B). Multinomial logistic regression
297 was used to assess the pseudo-temporal sample imbalance in individual lineages, while adjusting for
298 baseline sample probabilities. Macrophages from sham mice were more likely to be enriched further
299 along in the pseudotime trajectories of both prototypical and proliferative lineages, as expected due
300 to a greater replenishment post transient inflammation and were less likely to be present in the pro-
301 disease LpM lineage. Macrophages from vehicle treated mice were most abundant in the pro-disease
302 lineage and predominant across all pseudotime points indicating increased pro-disease differentiation
303 (Fig.5B). Conversely, in RRx-001 treated mice, macrophages were present at earlier pseudotime points
304 in the prototypical and proliferative lineages and were also less present in the pro-disease LpM
305 lineage, suggesting a reduction in pro-disease phenotypical differentiation. These data led us to
306 conclude that RRx-001 appears to prevent the acquisition of pro-disease phenotype. As our analysis
307 revealed pseudo temporal differences at early pseudotime points, we performed an aggregate
308 analysis of the LpM and SpM populations from RRx-001 and vehicle mice which also indicated
309 differences in SpM gene expression (Fig.5C). To further probe these differences, we performed gene
310 set enrichment analysis with ClusterProfiler using GO terms (RRx-001 vs Vehicle), and identified terms
311 related to activation of macrophages, antigen processing and defence responses (Fig.5D).
312 Furthermore, KEGG pathways suggested an enhancement of phagosome and lysosomal activity,
313 alongside antigen processing, with the majority activated in both the LpM and SpM populations (Fig.
314 5E), supporting the concept that treatment of induced endometriosis with RRx-001 may impact
315 peritoneal myeloid populations early in the differentiation trajectory. In line with RRx-001 enhancing
316 phagocytic activity in macrophage populations we demonstrated reduced average expression level of
317 Sirpα in transcriptomic and gene activity data (inferred from ATAC) compared to vehicle treated mice,
318 corresponding with our flow cytometric analysis at day 14 (Figs.5F, Fig.1H) and indicating that RRx-
319 001 acts to disrupt the Sirpα-CD47 immune evasion signal that is enhanced in endometriosis.
320 **The impacts of RRx-001 are specific to the endometriosis niche and peripheral blood.** 10x single cell
321 transcriptomic profiling was used to investigate the transcriptomic impacts of RRx-001 on all Cd45+
322 leukocytes isolated from the peripheral blood, endometrium, liver, lungs and spleen, to determine

323 peripheral immunological impacts and assess potential off-target effects in distal organs (Fig.6A).
324 Fluorescent activated cell sorting (FACs) was utilised to isolate Cd45+ leukocytes from RRx-001 and
325 vehicle treated mice in the 'menses' model of induced endometriosis, at day 14 post-lesion induction,
326 followed by processing of sorted cells using the 10x genomics chromium single cell platform to
327 generate transcriptomic libraries (n=4, n=4, respectively, Figs. 6A, S4A). An integrative UMAP
328 visualisation of matched samples from each tissue from RRx-001 and vehicle treated was performed
329 to enable visualisation of all 10909 cells (post quality control), revealing detection of all expected
330 leukocyte populations as per known marker gene expression, and some organ specific localisation of
331 cells (Fig.6B, 6C). Analysis of complexity score (log10GenesPerUMI) revealed consistency of
332 sequencing between both organs and condition(Fig. 6D).
333
334 We initially focussed our analysis on the peripheral blood, analysing samples from RRx-001 and vehicle
335 treated mice. Leukocyte populations identified according to canonical markers in the blood included
336 T cells (Cd4+ T, Tox+ T, Tregs, Cd8+ T, γδ T), natural killer cells (NK), B cells (B1, B2, and Pre-B), naïve
337 T/B cells, monocytes (inflammatory monocytes and patrolling monocytes) and a proliferative cluster
338 of immune cells (Fig.6E). An analysis of sample composition by cluster revealed all immune
339 populations were shared between experimental groups, with an increased abundance of Cd4+ T cells
340 expressing Ms4a6b, IL7R (naïve T cell marker) and IL6ra detected in RRx-001 treated mice (Fig.6F). We
341 performed gene set enrichment analysis with ClusterProfiler using GO terms (RRx-001 vs Vehicle) for
342 these expanded Cd4+ T cells, and identified terms related to metabolism, cytoplasmic translation and
343 oxidative phosphorylation, suggesting a metabolic activation of this population (Fig.6G). Monocytes
344 were of low abundance within the peripheral blood in both vehicle and RRx-001 treated mice; a trend
345 of reduced Mrc1 (Cd206) was seen in patrolling monocytes following RRx-001 treatment, as previously
346 reported in small cell carcinoma patients (Fig.6F, S4B)(*51*). We utilised CellChat to infer
347 communication networks within the peripheral blood in RRx-001 and vehicle treated mice, and to
348 probe condition specific signalling. CellChat also identified differential interaction strength in the cell-
349 cell communication network among peripheral leukocytes in RRx-001 treated mice, revealing the
350 highest differential outgoing signalling in inflammatory monocytes (Fig.6H). Probing the specific
351 signalling changes of inflammatory monocytes by comparing the outgoing and incoming interactions,
352 identified changes uniquely associated with RRx-001 treated mice in PECAM2, CCL and LAMININ
353 signalling, associated with trans-endothelial migration and concurrent with our observations of
354 increased monocyte-derived macrophages in the peritoneal fluid of these mice (Fig 6I).
355

356 To investigate any potential macrophage modulation in distal organs, we performed similar matched
357 analyses of leukocytes isolated from the endometrium, liver, lungs and spleen. In the endometrium,
358 UMAP visualisation was utilised for identification of leukocyte populations according to canonical
359 markers, revealing predominant macrophages (Mac/Mono, Mac/AP and Prolif Mac) and NK cells
360 (NK1/Cd4+ T cells, NK2 and NK3) (Fig.7A). All cell types were present in RRx-001 and vehicle treated
361 mice, with no impacts to immune cell composition detected (Fig.7B). We utilised differential gene
362 analysis (MAST) to analyse up and down-regulated genes in the Mac/Mono in RRx-001 compared to
363 vehicle control mice (Fig.7C) and minimal changes in gene expression were detected (<10 highlighted
364 DEGs), suggesting that RRx-001 does not modify endometrial macrophages. We repeated these
365 analyses in the liver, lungs and spleen. Immune cell composition was not altered across all distal
366 organs analysed and minimal modification of macrophage gene expression was observed (<5 DEGs)
367 (Fig.S4C-E).
368
369 **RRx-001 does not impact reproductive function in mice.** Our transcriptomic analysis revealed minimal
370 detectable impacts to the immune cell composition in distal tissues or modification of macrophages
371 in the endometrium and other organs. Moreover, the therapeutic activity of RRx-001 has been safely
372 evaluated in over 300 patients with no increase in infections or anaemia detected, indicating limited
373 side-effects. Impact on reproductive function has not yet been evaluated(*37*). Currently, gold-
374 standard treatment of endometriosis focuses on surgical intervention or therapeutic ovarian
375 suppression (oral contraceptives/GnRH agonists). A non-hormonal medical alternative that does not
376 interrupt reproductive function is urgently needed. To this end, we sought to determine if pre-
377 pregnancy treatment with RRx-001 led to any aberrant changes to fertility or developmental impacts
378 in mice. Pre-pregnancy intravenous dosing was chosen for these initial experiments as an RRx-001-
379 bound haemoglobin adduct persists for the lifetime of the red blood cell, reported to be 40.7 $\pm$ 1.9
380 (S.D) days in mice, potentially leading to long-term impacts(*52*). Tissue-resident endometrial
381 macrophages dynamically regulate tissue homeostasis and remodelling during the oestrous cycle in
382 mice(*53*), thus we initially investigated the impact of RRx-001 on oestrous cycle length, and within
383 individual stages, to identify any perturbations. Oestrous cycles were synchronised using the Whitten
384 effect(*54*), followed by daily staging by wet vaginal cytology preparations for > 4 complete cycles prior
385 to treatment with either RRx-001 or vehicle for 1-week. Daily staging continued for > 4 further cycles.
386 No significant changes in overall cycle length or individual cycle stage were detected in RRx-001
387 treated mice pre- or post-treatment (Fig.7D, E).
388 Next, mice were dosed with RRx-001 or vehicle for 1-week, with harem breeding set up 24-
389 hours post final drug dose for investigations into reproductive function. Within these experiments,

390 pregnancy success rates following copulatory plug detection were as expected within breeding
391 colonies: 13/16 RRx-001 treated mice became pregnant (1 did not plug, 2 not pregnant post-plug) and
392 14/15 vehicle treated mice became pregnant (1 not pregnant post-plug). Sexual receptivity was
393 assessed by daily seminal plug checks, detected between 0.5 - 4.5 days post-mating. No significant
394 differences in time to seminal plug were observed (Fig.7F). At embryonic day (E)10.5, no significant
395 differences in average embryo number or embryo weight were determined between experimental
396 groups (Fig.7G,H). At E15.5, Hofbauer cells, a heterogenous population of placental macrophages
397 which broadly exhibit a pro-repair phenotype, were isolated from the chorionic villus of the foetal
398 placenta and assessed using quantitative spectral flow cytometry (Fig.S5). We sought to assess
399 Hofbauer phenotype; dysregulation of these cells is associated with placental pathologies including
400 inadequate development, inflammation and infection(*55*). No significant differences were identified
401 in the MFIs of SIRPα, CD206 and CD40 between RRx-001 and vehicle groups (Fig.7I). As expected for a
402 predominantly pro-repair population, CD206 was expressed across both experimental groups, with no
403 expression of pro-inflammatory CD40.
404 Finally, the remaining pregnant mice and pups were monitored throughout pregnancy and
405 during the postnatal period. We found no impact of RRx-001 on gestational length (Fig.7J).
406 Furthermore, mice treated with RRx-001 did not have any alterations to number of pups (ranging from
407 2-11 in the vehicle group, and 3-11 in the RRx-001 treated group; Fig.7K), or sex ratio of litter (Fig.S5B).
408 Post parturition, mothers remained healthy and omental milk spots were observed in all pups on day
409 1 indicative of successful lactation and nursing. Pups were weighed at postnatal day 7, with weekly
410 weighing up to 28 days of age, with no significant differences detected at any timepoint (Fig.S5C).
411 Collectively, these data indicate that RRx-001 does not impact reproductive function.
412
413 **Discussion**
414 In the current study we have demonstrated that RRx-001 has a robust therapeutic impact in mouse
415 models of induced endometriosis; treatment decreased lesion number and size, and attenuated pain
416 associated behaviours. Our macrophage depletion study confirmed that the predominant mechanism
417 of action was via macrophages and that they are essential to mediate the therapeutic effect. In line
418 with this, using multiomic single nuclei sequencing we showed that RRx-001 impacted peritoneal
419 macrophage populations whereby the abundance of pro-disease macrophages was reduced, and the
420 proportion of pro-resolving macrophages was enhanced. Trajectory analysis inferred that RRx-001
421 tips the balance in favour of pro-resolving macrophage by preventing differentiation to a pro-disease
422 phenotype. Macrophage phenotype was not modified in other tissues, indicting specificity for the
423 endometriotic niche. Finally, preliminary investigations into reproductive function suggest that RRx-

424 001 does not impede fertility or aberrantly affect embryonic development *in utero.* Taken together,
425 we present promising preclinical data highlighting RRx-001 as a novel macrophage directed therapy
426 for the treatment of endometriosis.

427 In the 'menses' model of induced endometriosis we found that when treatment with RRx-001
428 was initiated prior to establishment of lesions, there was no difference in bioluminescent signal
429 between vehicle control and drug treated mice on day 3, indicating that RRx-001 does not impact the
430 initial stages of ectopic endometrial tissue adhesion within the peritoneal cavity. This aligns with the
431 proposed erythrophagoimmunotherapeutic activity of RRx-001; in which the covalent encapsulation
432 of RRx-001 in red blood cells vectors RRx-001 to hypoxic (tumour) vasculature – leading to vasculature
433 occlusion, haemolysis and erythrophagocytosis by tumour associated macrophages(*40*). This
434 phenomenon may also be occurring in lesions, which also exhibit hypoxic areas, following the initial
435 stages of vascularisation that occur in the first week(*56*). Interestingly, in the menses model, RRx-001
436 treatment led to a reduction in bioluminescent signal between days 3 to 7 and days 3 to 14, but not
437 day 3 to 10, this may be related to cases seen in the treatment of lung cancer with RRx-001, when
438 tumour pseudo-progression is detected early in treatment due to tumoral lymphocyte infiltration,
439 before regression occurs later, leading us to hypothesise that this may also be occurring within the
440 endometriotic lesions(*56*). Accordingly, when we investigated the impact of RRx-001 on established
441 lesions in the 'menses' model, we identified a reduction in bioluminescent signal whereas, co-
442 treatment of RRx-001 with liposomal clodronate (to deplete peritoneal macrophages) led to an
443 increase in bioluminescent signal. This highlights macrophages are crucial for the therapeutic efficacy
444 of RRx-001. Future studies should establish the dynamics of pseudo-progression, if present, and
445 determine the regime required for complete elimination of lesions.

446 We also investigated the impact of RRx-001 in a minimally invasive model of induced
447 endometriosis. We previously determined that endometriotic lesions established using this model
448 exhibit greater longevity(*38*). In this model, full thickness uterine fragments are transferred containing
449 myometrial tissue, resulting lesions are usually larger than in the menses model and have a cystic
450 appearance. We used two models in this study to represent different 'phenotypes' of endometriosis,
451 with the minimally invasive model representing a more persistent form of endometriosis, and
452 following the suggestions in the WERF EPHect guidelines for experimental models that encourage the
453 use of multiple models in preclinical testing (*41*). Here, we also demonstrated a significant reduction
454 in lesion growth when treatment was initiated 1-week post-lesion induction, rather that prior to lesion
455 induction, again indicative that RRx-001 resolves established lesions. In both models, treatment with
456 RRx-001 led to an attenuation of abdominal mechanical hyperalgesia, indicative of reduced pain in
457 this region and perhaps due to the accompanying resolution of lesions with treatment. We also

458 included non-evoked behavioural tests as they better recapitulate impacts to well-being that are
459 associated with endometriosis and are used as surrogate measures of visceral pain. The inclusion of
460 non-evoked behavioural tests were described recently as an absolute requirement in the replication
461 and translation of the complex pain experience of endometriosis patients(*43*). In our studies, nest
462 building(*57*) was the most sensitive assay for identifying behavioural phenotypes; impaired nest
463 building was seen in mice at day 7 post-lesion induction. Following treatment with RRx-001 nest
464 building was significantly improved beyond that observed in naïve, pre-endometriosis mice.

465 Depletion of macrophages by clodronate prevented RRx-001 from impacting endometriotic
466 lesions, demonstrating a critical role of macrophages in the anti-endometriosis activity of RRx-001.
467 This is consistent with data from oncology studies, in where RRx-001 has been shown to modulate
468 TAMs towards a pro-inflammatory state, with enhanced immune infiltration and vascular remodelling.
469 The presence of infiltrating macrophages was identified as a *sine qua non* condition for the anti-
470 tumour activity of RRx-001, with depletion of TAMs attenuating the impacts of RRx-001 in an A549
471 xenograft mouse model(*58*). This mechanism of macrophage modulation was reflected in the
472 multiomic analysis, highlighting that RRx-001 leads to a reduction in phenotypically pro-disease LpM
473 and an accumulation of a phenotypically polarised LpM, termed pro-resolving LpM (prototypical LpM
474 remained constant in each group (sham, RRx-001, vehicle). Trajectory analysis suggested that the pro-
475 resolving LpM phenotype is a transitory cell state, thus we predict that RRx-001 prevents the
476 acquisition of a pro-disease phenotype by newly recruited monocyte-derived LpM, and enhances the
477 continuous recruitment of monocytes to the peritoneal cavity. Our transcriptomic analysis supported
478 this hypothesis, identifying differential cell-cell communication in peripheral blood inflammatory
479 monocytes related to trans-endothelial migration following treatment with RRx-001, supporting the
480 hypothesis of increased recruitment and extravasation of circulatory monocytes into the peritoneal
481 cavity. This builds on previous observations of peripheral monocyte modulation in small cell carcinoma
482 patients receiving RRx-001, such as reduced expression of pro-tumorigenic CD206 (murine equivalent
483 Mrc1), with the same trend also detected in patrolling monocytes in mice that received RRx-001 within
484 this current study (*51*). In small cell carcinoma patients, downregulation of CD206 was positively
485 correlated with increased treatment response and survival, with our novel observation of enhanced
486 extravasation and recruitment of monocytes adding to the mechanistic understanding of beneficial
487 RRx-001 activity (*51*).

488 The transcriptional phenotype of pro-resolving LpM exhibited some similarities to that of
489 monocyte-derived LpM observed in our previous studies(*26*) which were attributed to protective
490 functions in the mouse model of endometriosis. DEGs include lipid associated genes and those
491 encoding C1q; suggesting roles in the reduction of available lipids, hormone synthesis and activation

492 of membrane lytic complexes. In patients with endometriosis, lipidomic studies have highlighted
493 dysregulated lipid metabolism and elevated levels of certain lipid species, possibly driven by oxidation
494 stress and inflammation in the body, suggesting a potentially beneficial effect of enhancing lipid
495 metabolism and warranting further investigation in endometriosis research (*59, 60*). C1q, the initiator
496 of the classical complement pathway, places a multifaceted role in immune surveillance, inflammation
497 and tissue remodelling, processes all relevant to the pathophysiology of endometriosis. We observed
498 enhanced C1q following RRx-001 treatment, which may promote the clearance of ectopic endometrial
499 cells by facilitating the opsonization and removal of apoptotic cells and their cellular debris, while
500 concurrently suppressing inflammasome activation, thus controlling peritoneal inflammation. Similar
501 protective effects have been reported in early atherosclerotic lesions, a disease which shares many
502 commonalities in the involvement of macrophages and inflammatory pathways; complement
503 activation via C1q has been identified as protective in early lesions by dampening inflammation,
504 benefits which diminish at later disease stages (*61, 62*). Concurrently, the pro-angiogenic and immune-
505 evasive properties of C1q may contribute to pathological angiogenesis and persistence of established
506 lesions at later timepoints, indicating its role may be time-dependent in the progression of the disease
507 and suggesting the need for temporally informed immune modulation strategies in endometriosis
508 (*63*). Treatment with RRx-001 also appeared to increase genes associated with response to pathogens
509 and antigens, again suggesting improved visibility of ectopic tissue to peritoneal macrophages and
510 potentially enhanced clearance of apoptotic debris. Together these modifications to peritoneal
511 macrophages may reduce endometriosis drivers and promote destruction of ectopic tissue.

512 RRx-001 has previously been shown to have significant impacts on the epigenome of cancer
513 cells; effects vary depending on the dose and timepoints evaluated. Sites that were hypo- and hyper-
514 methylated as well as globally increased acetylation were reported(*64*). We predict that in the
515 peritoneal cavity RRx-001 prevents acquisition of pro-disease phenotype via epigenetic modification.
516 Of particular interest, we found that Klf (including Klf14) binding motifs were enriched in peritoneal
517 macrophages derived from mice exposed to RRx-001. Previous studies have identified a role for Klf14
518 in reducing glucose metabolism and immune function in macrophages; this seems to exert a protective
519 function in inflammatory conditions by limiting inflammatory cytokine secretion(*49*). Further studies
520 should validate these findings mechanistically. These modifications also highlight the paradoxical
521 nature of RRx-001 mechanisms reported in the literature, whereby antigenicity is enhanced whilst
522 simultaneously promoting an antioxidative and anti-inflammatory environment (*65*).

523 Much of the research conducted on the mechanism of action of RRx-001 has occurred in the
524 oncology field, where studies describe targeting of RRx-001 to hypoxic and aberrant vasculature
525 prevalent within tumours via binding to haemoglobin within red blood cells. Drug bound RBCs travel

526 to hypoxic vasculature where they accumulate because of their RRx-001 induced rigidity(*66*). During
527 this process, nitric oxide (NO) is released which is thought to confer cytotoxic activity within
528 tumours(*67*). Macrophages also engulf RRx-001 bound RBCs, inducing polarisation from a pro-repair
529 to pro-inflammatory state and down-regulating the CD47-SIRPα pathway, which reduces tumour cell
530 immune evasion(*68, 69*). Immunogenicity of cancer cells is also induced via increased expression of
531 interferon (IFN)-responsive genes(*70*). Given the similarities that exist between cancer and
532 endometriosis (including pro-disease macrophage polarisation and pathological immunotolerance)
533 and that endometriosis lesions also exhibit a hypoxic environment, we predict that significant RRx-001
534 impacts are also occurring within lesions. In support of this, the transcriptomic analyses performed in
535 this study infer such a targeted mechanism, as we detected profound immunological changes only in
536 the peritoneal fluid with a fine tuning of the systemic immunity identified in peripheral blood. Future
537 work will interrogate the intra-lesional environment in response to RRx-001. In the current study, we
538 failed to evaluate this as the lesions recovered were so reduced in size that we were unable to recover
539 enough cells for scRNA-Seq studies on multiple occasions. The mediation of indirect effects within
540 associated environments has not yet been characterized, however from our results it is plausible to
541 suggest that the modulation of macrophage populations within the peritoneal cavity occurs as a
542 secondary outcome resulting from endometriotic lesion resolution by lesion-resident macrophages
543 and a subsequent reduction in the signals that dictate the acquisition of a pro-disease LpM
544 phenotype, or by reactivating a previously immunotolerant microenvironment within the peritoneal
545 cavity. The release of reactive oxygen and nitrogen species may also play a role. Thus, further work is
546 required to elucidate the impacts of RRx-001 on lesion-resident macrophage populations.
547
548 To investigate potential impacts on fertility, we evaluated the endometrium immune
549 environment and reproductive parameters in mice exposed to RRx-001. Our findings suggest that
550 RRx-001 does not impact the immune cell composition within the endometrium or modify
551 endometrial macrophage gene expression. Additionally, pre-pregnancy treatment with RRx-001 does
552 not impair the normal reproductive function of female mice or embryo development indicating that it
553 has potential suitability as a non-hormonal and fertility sparing treatment for endometriosis. Further
554 work will identify whether RRx-001 can rescue endometriosis-associated infertility.
555 To summarize, we have revealed a novel indication for the anti-cancer drug RRx-001 in the
556 treatment of endometriosis. It acts to reduce endometriosis lesions, associated pain-like behaviours
557 and modulates macrophage populations in the peritoneal cavity without negatively impacting fertility
558 or modifying macrophages in distal tissues. RRx-001 is currently in phase I - III clinical trials for different
559 solid cancers, is well tolerated with available safety data. In this first phase of preclinical testing, we

560 highlight a robust effect in experimental endometriosis and plan to proceed to a feasibility trial in
561 women with the disorder. RRx-001 and its macrophage modifying actions has the potential to improve
562 the lives of millions of women suffering from endometriosis.
563
564 **Acknowledgements**. The authors thank Dr Laura Baxter at the Bioinformatics RTP, University of
565 Warwick, for pre-processing of multiomic data; the Biological Services Unit, University of Warwick, for
566 care of mice; and the FlowSRL, University of Warwick, for assistance with flow cytometry experiments.
567 We would also like to thank Deborah McIntyre for the independent quantitative scoring of nests.
568
569 **Funding**. This work was supported by an MRC iCASE (Ferring Pharmaceuticals were the industrial
570 partner and provided additional funding for consumables and travel) studentship to I.M and an MRC
571 Project Grant (MR/S002456) to E.G. The authors declare no conflict of interest.
572
573 **Author contributions:** E.G conceptualised and supervised the study and acquired funding. I.M
574 conducted all experiments, analysed data, and performed multiomic and transcriptomic analyses. V.V
575 performed multiomic analyses. C.L.P and M.R performed experiments. P.D and K.P performed animal
576 experiments. I.M and E.G wrote the manuscript.
577
578 **Data and materials availability:** All data associated with this study is present within the manuscript
579 and the included supplementary materials. Analysis script for multiomic and transcriptomic analyses
580 are publicly available on github.com under project tbc. Multiomic sequencing data are deposited in
581 Gene Expression Omnibus under accession number tbc.
582
583 **Materials and Methods**
584 **Study design**. Experiments were designed to determine the impact of RRx-001 treatment in a mouse
585 model of experimental endometriosis and to identify any potential impact on fertility outcomes. For
586 the purpose of determining the impact of RRx-001 on induced endometriosis, we implemented two
587 complementary mouse models ('menses'(*71*) and 'minimally-invasive'(*38*)) in which to robustly
588 examine endometriotic lesion growth and pain-like behaviours. A macrophage depletion study in the
589 'menses' model allowed us to confirm the effects seen were mediated by peritoneal macrophages.
590 Additionally, we utilised multiomic sequencing to determine transcriptomic and epigenomic effects of
591 RRx-001 on peritoneal macrophages isolated from the 'menses' mouse model, and single cell
592 transcriptomic sequencing of Cd45+ leukocytes isolated from the peritoneal fluid, peripheral blood
593 and distal organs (liver, lung, spleen and endometrium) to assess cell-cell communication and

594 potential off-target impacts. To assess fertility outcomes, we examined the effect of pre-pregnancy
595 dosing of RRx-001 on the oestrous cycle and reproductive functions. Animals were randomised to
596 either RRx-001 treatment or control groups using the GraphPad QuickCalcs online tool
597 (https://www.graphpad.com/quickcalcs/randomize1/). Behavioural experiments were performed
598 under blinded conditions. Details of mouse models, sample size and statistical methods are described
599 in the appropriate sections below.
600
601 **Animals**. Wild-type FVB/N mice were purchased from either Envigo (Cambridge, UK) or Charles River
602 (UK) and maintained under standard conditions at the University of Warwick, UK. FVB-Tg(CAG-luc,-
603 GFP)L2G85Chco/J (stock number 008450|L2G85) were originally purchased from The Jackson
604 Laboratory (Bar Harbor, ME, USA), and a breeding colony maintained under standard conditions at
605 the University of Warwick. Mice were housed in standard conditions with a 12:12 light-dark cycle, an
606 ambient temperature of 21°C, humidity at 50%, and *ad libitum* access to food (standard rodent chow)
607 and water. The diet of weanlings was supplemented by apple sauce. Following arrival to the facility,
608 mice acclimatised for one week prior to commencement of experimental procedures. All procedures
609 performed were permitted under license by the United Kingdom Home Office Animal Experimentation
610 (Scientific Procedures) Act; PPL PP0568394, and in accordance with the guidelines of the Committee
611 for Research and Ethical Issues of the International Association for the Study of Pain.
612
613 **Mouse models of experimental endometriosis.** We implemented two variations of the
614 bioluminescent syngeneic mouse models of induced endometriosis; a 'menses' model and a minimally
615 invasive model, described in detail previously(*38, 71*). In brief, for the 'menses' model, recipient FVB/N
616 mice (n=40) were ovariectomised and received an intraperitoneal injection of decidualised and
617 progesterone withdrawn donor endometrium (*72*) recovered from FVB/Cag-Luc mice (~40mg, minced,
618 combined, resuspended in saline and passed through an 18 g needle; n = 40 FVB/Cag-Luc donors) and
619 exogenous oestradiol supplementation (oestradiol valerate 500 ng, twice weekly). Surgical controls,
620 referred to as 'sham' mice, were ovariectomised FVB/N mice that received intraperitoneal injection
621 of saline instead of tissue. In the minimally invasive model, intact recipient FVB/N mice (n = 32)
622 received an intraperitoneal injection of FVB/Cag-Luc donor full-thickness uterus (equivalent to 1
623 uterine horn per recipient, minced and passed through an 18 g needle; n = 16 FVB/Cag-Luc donors).
624 Oestrus stage was determined in donors and recipients by vaginal smear and retrospective cytological
625 analysis(*73*).
626
627 **Experimental groups**.

628 Mice were randomly assigned to either (I) RRx-001 treatment, (II) vehicle control, (III) RRx-
629 001+clodronate group, (IV) sham or (V) naïve (no procedures). Experimental groups included in each
630 experiment are as tabulated below. During these experiments, 5 mice were culled early due to adverse
631 effects (venous irritation of tail) and were not included in reported numbers or data. Dosing schedules
632 are noted in individual experimental schematics. In all our studies, RRx-001 (Selleck Chemicals, USA)
633 was dosed intravenously at 10mg/kg in DMA:PEG-400 1:2, diluted 1:4 in sterile saline immediately
634 prior to injection, 2x weekly (Monday and Thursday, 12pm), with control mice receiving vehicle
635 (DMA:PEG-400 1:2) only.
636

Experiment	Model of induced endometriosis	Groups included
Bioluminescent monitoring of lesions	Menses; pre-treatment	I (n=13), II (n=11), V (n=3)
	Minimally invasive; post-establishment	I (n=16), II (n =16)
Clodronate depletion	Menses; post-establishment	I (n=5), III (n=6)
10x Multiome	Menses; pre-treatment	I (n=9), II (n=5), IV (n=3)
10x GEX	Menses; pre-treatment	I (n=4), II (n=4)
Fertility	N/A	I (n=20), II (n=18)

637
638 **Non-invasive *in vivo* bioluminescence quantification**. As described previously(*39*), mice were injected
639 subcutaneously with 1.5 mg D-Luciferin Potassium Salt (75mg/kg, reconstituted in sterile PBS and
640 sterilised by 0.22 µm filtration), following a 5-minute period to allow a maximal luciferase signal
641 plateau, mice were imaged under maintained anaesthesia using a PhotonIMAGER (Biospace Lab,
642 Paris)(*38*). Lesion bioluminescence was measured using a standard region of interest across
643 experiments, on the front and back of each mouse for 7 minutes per side. Using M3 Vision software
644 (Biospace Lab), the background reading was subtracted, front and back readings averaged, and
645 photons/s/cm2/sr calculated for bioluminescent signal quantification.
646
647 **Histological and ImageJ analyses**. Post tissue fixation and embedding in paraffin, 3 µM sections of
648 recovered lesions were stained using a standard haematoxylin/eosin protocol. Images were taken on
649 a LeicaDMI microscope (Leica, Germany), with white balance and histological verification of
650 endometriotic lesion hallmarks (stroma +/- glandular epithelium) conducted in FIJI (ImageJ2, Version
651 2.3.0). In FIJI, analysis to determine cross-sectional area was performed on lesion images captured
652 using 4x magnification, image scale was set to a known size and the 'select' tool was implemented to
653 outline the lesion while excluding peritoneal wall/adipose tissue, and the 'measure' function was then
654 used to calculate cross-sectional lesion area.

655

656 **Behavioural assessments**.

657 *von Frey*. We determined mechanical allodynia as an average of measurements taken on days
658 11/12/13 post lesion induction ('menses' model) or day -1 (baseline), 8 (1 week; initiation of
659 treatment) and 18 (10 days following start of treatment; minimally invasive model) using calibrated
660 Semmes-Weinstein von Frey filaments (Stoelting, Wood Vale, IL, USA), as described previously(*38, 74*).
661 Briefly, mice were allowed to adapt to the apparatus until exploratory responses ceased. Filaments
662 were then applied 10 times in ascending order to the abdomen or hind paw. The filament force
663 (grams) was recorded when withdrawal responses were observed in 50% of applications.

664 *Hot plate.* Thermal hyperalgesia was determined prior to lesion induction, and on day 7 and day 17
665 post-lesion induction using a hot plate (Ugo Basile, Italy). Mice were positioned onto a preheated plate
666 set at 52°C and their responses were observed. A time-to response (seconds) was noted when mice
667 exhibited a reaction to the thermal stimulus. If no response was observed within 25 seconds, the mice
668 were removed from the plate.

669 *Thermal plate preference.* Thermal hyperalgesia was determined prior to lesion induction, and on day
670 7 and day 17 post-lesion induction using TPP thermal place preference plates (Ugo Basile, Italy). The
671 thermal plates were set at distinct temperatures, one at 12.5°C and the other at 30°C. Mice were
672 allowed a 15-minute-period for exploration of both plates, during which the duration spent at 12.5°C
673 was recorded.

674 *Burrowing.* The ethological rodent behaviour of burrowing was determined prior to lesion induction
675 and on day 8 and day 18 post-lesion induction. Mice were individually supplied with a burrowing tube
676 (diameter 6.8 cm, length 20 cm), made of clear acrylic, open and elevated by 3 cm at one end to
677 prevent the accidental displacement of burrowing substrate (tubes manufactured at Life Sciences,
678 University of Warwick). The mouse was placed in a plastic cage with the burrowing tube filled with
679 110g of wooden shredding; following a one-hour burrowing assay, the material remaining was
680 weighed and recorded, and the percentage of material displaced within an hour calculated.

681 *Nesting.* Nesting (also ethological) was determined prior to lesion induction and on day 8 and day 18
682 post-lesion induction as described(*57*). Briefly, 1 hour prior to dark phase, mice were individually
683 housed with wooden shredding and a Nestlet (VetTech, UK). The following morning, the nest was
684 imaged, and the quality of the nest created from the shredded nestlet recorded with a rating scale of
685 1-5. (e.g. 1 no nest; 5 fully shredded material arranged into a neat nest). Mice had *ad libitum* access
686 to food and water during the test and were re-grouped immediately following the nesting assay (Table
687 S1).

688

689 **Flow cytometry**. Peritoneal lavage was collected into 5 ml of ice-cold DMEM, red blood cells were
690 lysed (Red blood cell lysis buffer, Miltenyi Biotech) and cells filtered through a 40 µM filter and then
691 blocked with monocyte block (TrueStain Monocyte Blocker™ BioLegend), prior to resuspension and
692 staining of 1 million cells per sample with the antibody panel shown. Samples were analysed using a
693 FACS Aria Fusion with FACS Chorus software (BD Biosciences) and FlowJo v.9 software. Hofbauer cells
694 were isolated from the foetal placenta of mouse embryos at E15.5. Dissection of the foetal placenta
695 from embryonic yolk sacs and subsequent placental digestion into a single cell suspension were
696 performed as described previously, with three foetal placentas pooled from each mouse(*75, 76*).
697 Samples were filtered, RBCs lysed, blocked, and resuspended as above, prior to staining of 1 million
698 cells per sample with the antibody panel. Samples were analysed on a Sony spectral ID7000 spectral
699 cytometer (Sony Biotechnology, USA).
700

Marker	Fluorophore	Clone	Supplier	Product Number
CD45	Pacific Blue	30-F11	Biolegend	103125
Sirpα	BV510	P84	Biolegend	144005
Ly6C	BV711	HK1.4	Biolegend	128037
CD40	FITC	3/23	Biolegend	124607
c-kit	PerCP Cy5.5	ACK2	Biolegend	135133
CD163	PE	S15049F	Biolegend	156703
CD34	PE-Cy5	MEC14.7	Biolegend	119311
CD206	PE-Cy7	C068C2	Biolegend	141719
Lineage exclusion	APC		Biolegend	
CD19		1D3/CD19		152410
CD3		17A2		100235
CD335		29A1.4		137607
Ly6G		1A8		127613
SiglecF		S17007L		155507
MHCII	APC-Cy7	M5/114.15.2	Biolegend	107627
F4/80	APC Fire750	BM8	Biolegend	123117
Live/Dead	Zombie UV	-	Biolegend	423107

701
702 **Preparation of peritoneal immune cells for 10X multiomic sequencing**. Peritoneal lavage was pooled
703 within experimental groups (endometriosis/RRx-001 n=9, endometriosis/vehicle n=5, and sham n=3)
704 prior to processing and staining as described above, with fluorescence activated cell sorting based on

705 surface marker expression (Lin-/Cd45+) performed to enrich samples for macrophage populations.
706 100,000 cells per sample were sorted into 1ml PBS + 2% FBS using a FACs Aria. Gentle nuclei isolation
707 was performed, and nuclei were then processed and barcoded according to the established pipelines
708 to generate individual paired RNA and ATAC libraries using a 10x Nuclei Isolation Kit, a 10x Multiome
709 Kit and 10x Chromium Controller™ (10x Genomics). Libraries were sequenced individually by the
710 Genomics Lab at the University of Warwick on high-output 150 cycle cartridges using a NextSeq
711 500/550 (Illumina®, San Diego, USA).
712
713 **Preparation of leukocytes for 10X single cell sequencing**. All samples were pooled within
714 experimental groups (endometriosis/RRx-001 n=4 and endometriosis/vehicle n=4). Peritoneal fluid
715 was processed and stained as described above. Peripheral blood was collected via cardiac puncture,
716 prior to processing and staining as above. Mechanical disruption was used to prepare the spleen, prior
717 to processing and staining as above. Endometrial, liver, and lung tissues were digested for 20 minutes,
718 45 minutes, and 60 minutes, respectively, in 3 ml of a solution containing Collagenase IV (0.2 mg/mL)
719 and DNase I (0.05 mg/mL) in RPMI1640 at 37°C, prior to processing and staining as above.
720 Fluorescence activated cell sorting based on surface marker expression (Cd45+) was then performed
721 to isolate leukocytes. 100,000 cells per sample were sorted into 1ml PBS + 2% FBS using a FACs Aria.
722 Sorted cells were then processed using a 10x Chromium Next GEM Single Cell 3' Kit v3.1, and the 10x
723 Chromium Controller™ (10x Genomics) to generate transcriptomic libraries. Libraries were sequenced
724 by Novogene (Novogene Co., Ltd).
725
726 **Bioinformatic analysis of peritoneal multiomic data**. We followed recent guideline best practices for
727 single cell analysis across modalities as described by Heumos et al for our paired analysis of snRNA-
728 seq and snATAC-seq libraries(*77*). BCL files for each flow cell directory from the ATAC and GEX
729 sequencing runs were demultiplexed using Cell Ranger ARC analysis pipelines to generate FASTQ files.
730 Seurat (5.0.3) and Signac (1.13.0) in R studio (4.3.2) were used to create Seurat objects (v3) based on
731 GEX data, with ATAC-seq data added as a second assay. Using ATAC-seq data, a common peak set was
732 created and peaks were called in individual samples using MACS2 v2, with peaks on non-standard
733 chromosomes and in genomic blacklist regions removed(*78*). Independent quality filtering of each
734 dataset was performed on both modalities to remove low-quality cells based on number of detected
735 molecules for each modality, the number of genes detected per UMI, nucleosome signal and TSS
736 enrichment. As described in datasets generated by Yoshimura et al and 10x Genomics, the gentle
737 nuclei isolation protocol allows mitochondria to attach to the nuclei prior to GEM generation resulting
738 in a high mitochondrial percentage(*79*). Post-matrix generation we filtered reads aligned to

739 mitochondrial or ribosomal regions, and matrices were then subset on common genes. Finally, the
740 scDblFinder and SoupX were used to identify and remove doublets and assess ambient contamination,
741 respectively(*80, 81*). Pre-processing of RNA datasets was performed using the SCTransform v1
742 workflow (Seurat), followed by conservative anchor-based RPCA-integration using the default
743 k.anchor parameter (5) to align populations (Seurat). We then computed the LSI of individual peak
744 datasets using standard functionalities (Signac), followed by Harmony integration of datasets(*82*). The
745 Seurat v4 weighted nearest neighbour (WNN) method of 'FindMultiModalNeighbors' was utilised to
746 compute a joint neighbour graph to represent both the GEX and ATAC modalities, followed by the use
747 of standard workflows for WNN UMAP visualisation and clustering (Seurat). Clusters were identified
748 using marker genes identified in Wilcoxon rank-sum tests in a one-vs-all fashion for manual annotation
749 according to our previously published annotations of mouse peritoneal macrophages(*26*). Clusters
750 corresponding to non-macrophage populations or expressing < 1% of total cells were removed in order
751 to isolate 11,877 peritoneal macrophages (Fig.S3B, C). To account for within-sample correlation we
752 implemented MAST, a generalised mixed effect model, for differential gene expression testing(*83*).
753 Differentially accessible peaks were identified utilising logistic regression within the Signac
754 'FindMarkers' function. DNA sequence motif information (JASPAR2020) was added using the
755 'AddMotifs' function, with enriched motifs identified using 'FindMotifs'.
756 For data visualisation purposes the Seurat and Signac functionalities 'DimPlot', 'FeaturePlot',
757 'DotPlot', 'CoveragePlot', 'CellScatter', 'VlnPlot', 'MotifPlot', and the EnhancedVolcano package were
758 implemented(*84*) (*85, 86*). The clusterProfiler package was used for statistical analysis, output
759 simplification and visualisation of GO and KEGG terms(*87*). For trajectory analysis, DynGuidelines was
760 utilised to select the most applicable package and the indicated Slingshot package were
761 implemented(*88, 89*).
762
763 **Bioinformatic analysis of leukocyte transcriptomic data**.
764 BCL files for each flow cell directory from the GEX sequencing runs were demultiplexed using Cell
765 Ranger analysis pipelines to generate FASTQ files. BCL files for each flow cell directory from the GEX
766 sequencing runs were demultiplexed using Cell Ranger analysis pipelines to generate FASTQ files.
767 Seurat (5.3.0) was utilised in R studio to create Seurat objects (v5) based on filtered feature count
768 matrices. Independent quality filtering of each sample was performed to remove low-quality cells
769 based on percentage of mitochondrial reads, complexity (log10GenesPerUMI > 0.8), number of genes
770 and UMI counts. Merged objects of paired data from RRx-001 and vehicle treated mice were created
771 in each tissue type (endometrium, blood, lungs, liver and spleen) for further analysis. Standard Seurat
772 workflow of 'NormalizeData', 'FindVariableFeatures', 'ScaleData', 'RunPCA', 'FindNeighbours' and

773 'FindClusters' (SLM algorithm) was performed, with RunUMAP utilised for UMAP visualisation of
774 clusters. Clusters with no expression of CD45+ were removed from Seurat objects. Clusters were
775 identified and manually annotated according to marker genes identified using Wilcoxon rank-sum
776 tests in a one-vs-all fashion. Data visualisation was performed using the Seurat 'DimPlot' and scPubr
777 'do_ViolinPlot' functions (*90*). For differential gene expression testing between RRx-001 and vehicle
778 samples, we implemented MAST, a generalised mixed effect model, with data visualisation using
779 EnhancedVolcano. Paired datasets were combined from all organs and integrated using Harmony,
780 followed by visualisation using UMAP. The clusterProlifer and CellChat packages were utilised for
781 statistical analysis, output simplification and visualisation of GO terms, and to infer and visualise
782 differential cell-cell communication networks, respectively (*91*).
783
784 **Statistics**
785 Statistical analyses were performed using GraphPad Prism 10.1.1 for macOS (San Diego, CA). All
786 graphical data plotted as mean with standard deviation. For data meeting the necessary assumptions
787 for parametric analyses (Shapiro-Wilk), Student's t-tests or two-way analysis of variance (ANOVA) with
788 post hoc testing conducted with the Bonferroni test. If non-normality of data was detected, non-
789 parametric analyses were performed using a Mann-Whitney *U* test. Statistical significance for all tests
790 was established at $P < 0.05$. Significance levels were denoted as follows: * $P < 0.05$, ** $P < 0.01$, *** P
791 < 0.001, **** $P < 0.0001$.
792
793
794
795
796
797
798
799
800
801
802
803
804
805
806

807 **Figures and legends**

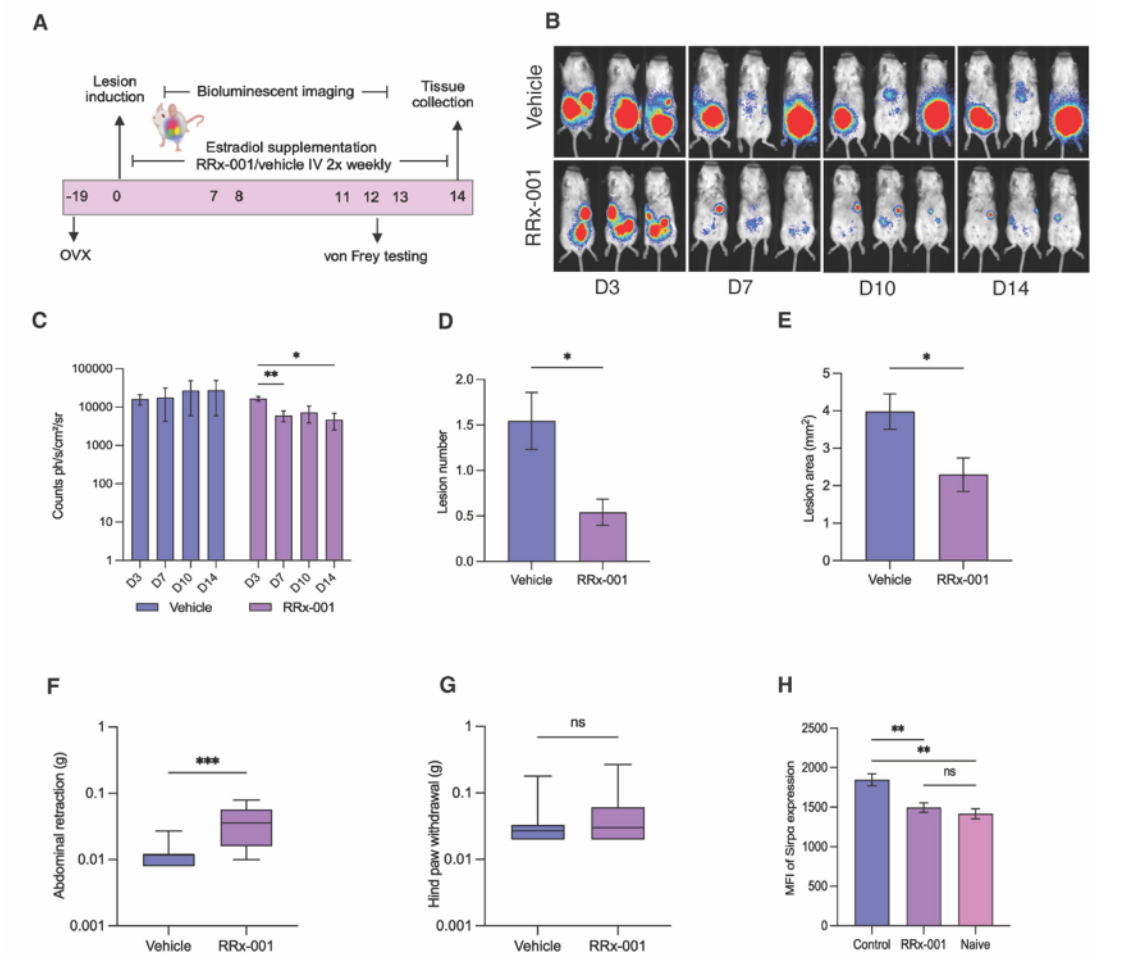

808

809 **Figure 1. RRx-001 reduces lesion growth and mechanical allodynia in a 'menses' model of**
810 **experimental endometriosis**. (A) Schematic of experimental design. (B) Representative images from
811 days 3, 7, 10 and 14 from RRx-001 and vehicle treated mice. (C) Quantification of lesion
812 bioluminescent signal of RRx-001 and vehicle treated mice with endometriosis; statistical analysis
813 performed using a two-way ANOVA with Bonferroni post hoc. (D) Number of lesions and (E) size of
814 lesions recovered from RRx-001 and vehicle mice; statistical analyses performed using a Mann-
815 Whitney test. (F) Mechanical hyperalgesia measured using von Frey filaments applied to the abdomen
816 and (G) hind paw (F and G plotted as an average of 3 measurements taken over days 11-13 post-
817 endometriosis induction). Statistical analyses performed using a Mann-Whitney test. (H) Median
818 fluorescence intensity (MFI) of Sirpα on large peritoneal macrophages; statistical analysis performed
819 using a one-way ANOVA. * $p < 0.05$, ** $p < 0.01$, **** $p < 0.001$.

820

821

822

823

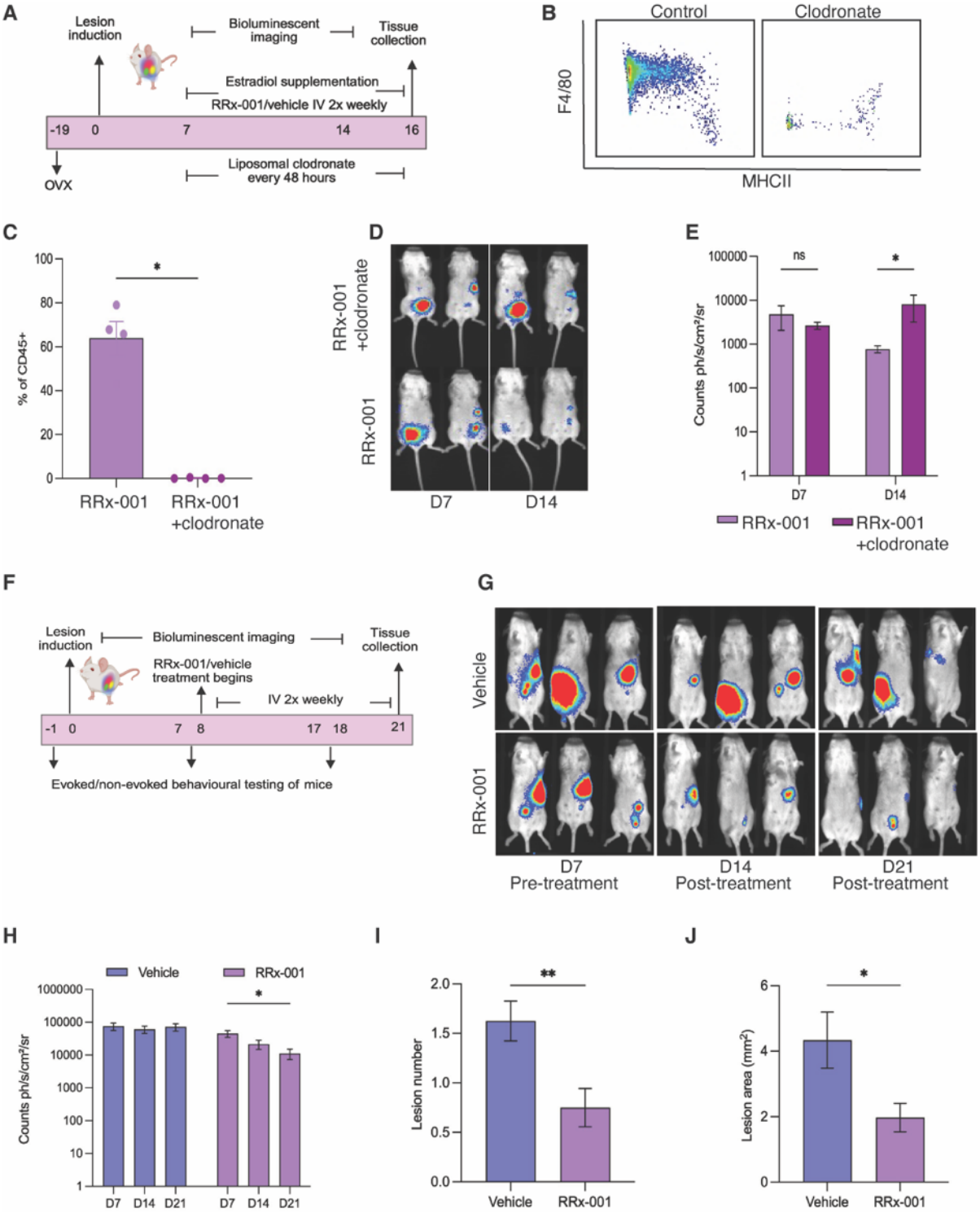

Figure 2. The macrophage-mediated therapeutic impact of RRx-001 on established endometriotic lesions in the menses and minimally invasive model of induced endometriosis. (A) Schematic of experimental design for combined RRx-001 treatment and clodronate depletion in the 'menses' model. (B) Representative flow cytometry plots of F4/80^{+} peritoneal macrophages from RRx-001 and RRx-001+clodronate treated mice, gated as in Fig.S2E. (C) Percentage of F4/80^{+} macrophages in the Lin^{-} CD45^{+} cells. (D) Representative images from days 7 and 14 from RRx-001 and RRx-001+clodronate

831 treated mice. (E) Quantification of bioluminescent signal of RRx-001 and RRx-001+clodronate treated
832 mice; statistical analysis performed using multiple Mann-Whitney tests with Bonferroni-Dunn
833 correction for multiple comparisons. (F) Schematic of experimental design for post-treatment in the
834 minimally invasive model. (G) Representative images from days 7, 14 and 21 from RRx-001 and vehicle
835 treated mice. (H) Quantification of bioluminescent signal of RRx-001 and vehicle treated mice;
836 statistical analysis performed using a two-way ANOVA with Bonferroni post hoc. (I) Number of lesions
837 and (J) size of lesions recovered from RRx-001 and vehicle mice; statistical analyses performed using
838 a Mann-Whitney test. * $p < 0.05$, ** $p < 0.01$.

839
840
841
842
843
844
845
846
847
848
849

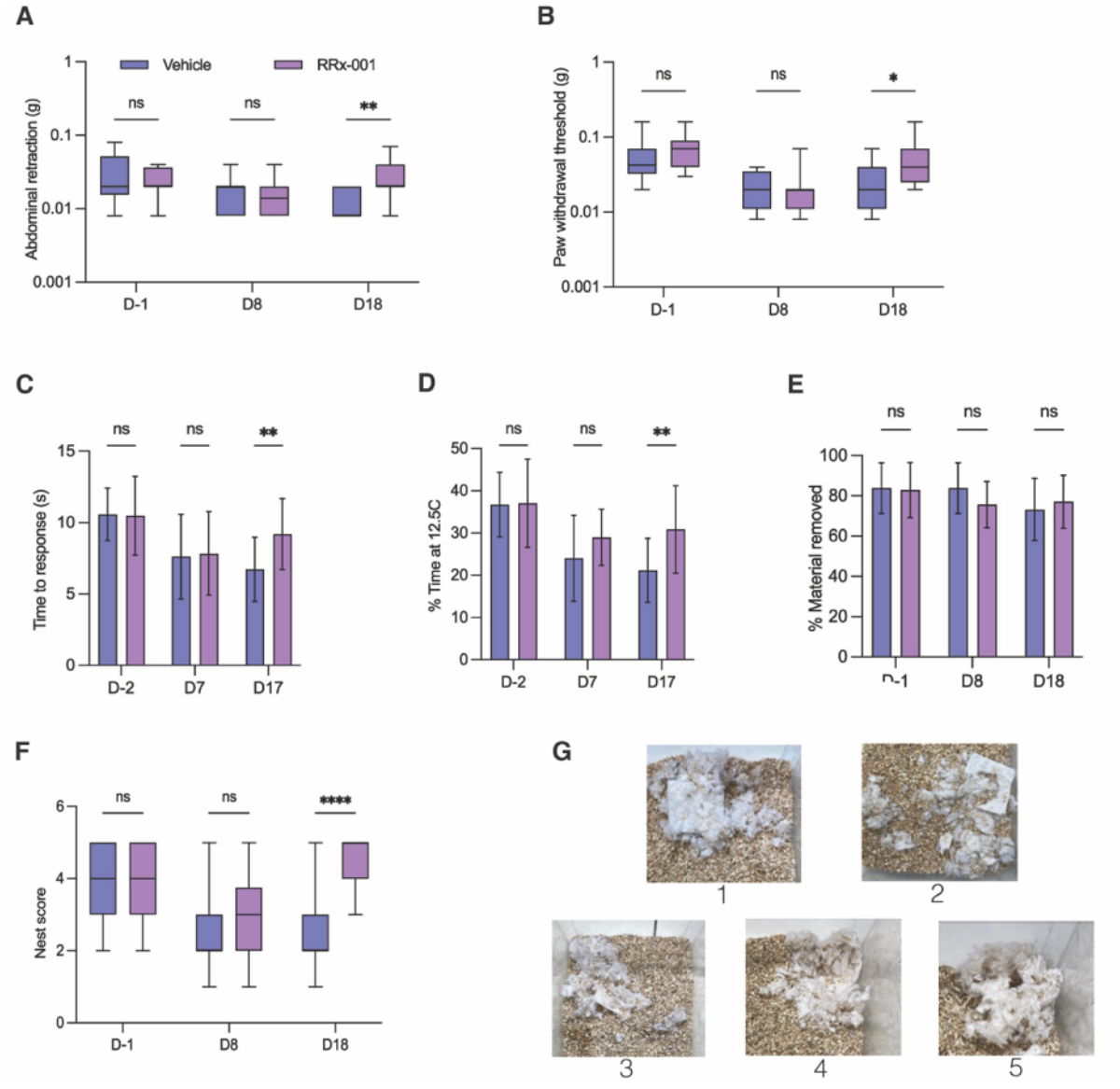

Figure 3. RRx-001 reduces evoked and non-evoked pain-associated behaviours in a minimally invasive model of induced endometriosis. (A) Mechanical allodynia measured using von Frey filaments applied to the abdomen and (B) hind paw; statistical analyses performed using multiple Mann-Whitney tests. (C) Hot plate latency assessed at 52°C; statistical analyses performed using multiple unpaired t-tests. (D) Percentage of material displaced in a burrowing assay; statistical analyses performed using multiple unpaired t-tests. (E) Thermal plate preference test analysis of % time spent on the 12.5 °C plate; statistical analyses performed using multiple unpaired t-tests. (F) Nest complexity scores; statistical analyses performed using multiple unpaired t-tests. (G) Example nests corresponding to scores 1-5. * $p < 0.05$, ** $p < 0.01$, **** $p < 0.0001$.

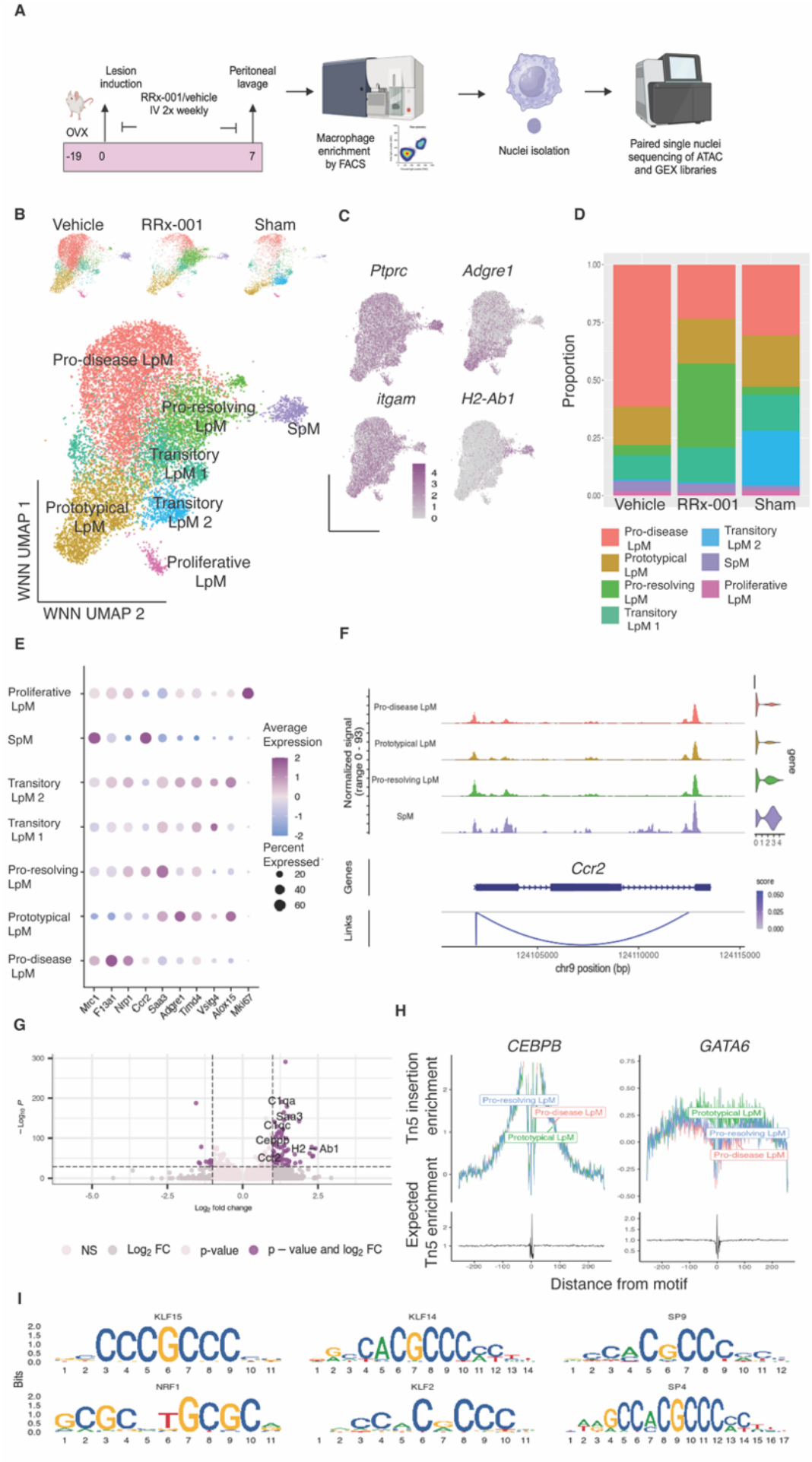
A
Lesion induction
Peritoneal lavage
RRx-001/vehicle IV 2x weekly
OVX
-19
0
7
Macrophage enrichment by FACS
Nuclei isolation
Paired single nuclei sequencing of ATAC and GEX libraries
B
Vehicle
RRx-001
Sham
Pro-disease LpM
Pro-resolving LpM
SpM
Transitory LpM 1
Prototypical LpM
Transitory LpM 2
Proliferative LpM
WNN UMAP 1
WNN UMAP 2
C
Ptprc
Adgre1
itgam
H2-Ab1
D
Proportion
Vehicle
RRx-001
Sham
Pro-disease LpM
Prototypical LpM
Pro-resolving LpM
Transitory LpM 1
Transitory LpM 2
SpM
Proliferative LpM
E
Proliferative LpM
SpM
Transitory LpM 2
Transitory LpM 1
Pro-resolving LpM
Prototypical LpM
Pro-disease LpM
Mrc1
F13a1
Nrp1
Ccr2
Saa3
Adgre1
Timd4
Vsig4
Alox15
Mki67
Average Expression
Percent Expressed
F
Normalized signal (range 0 - 93)
Pro-disease LpM
Prototypical LpM
Pro-resolving LpM
SpM
gene
Genes
Ccr2
Links
score
chr9 position (bp)
G
C1qa
Saa3
C1qc
Cebpb
H2-Ab1
Ccr2
Log2 fold change
NS
Log2 FC
p-value
p – value and log2 FC
H
CEBPB
GATA6
Tn5 insertion enrichment
Expected Tn5 enrichment
Pro-resolving LpM
Pro-disease LpM
Prototypical LpM
Distance from motif
I
KLF15
KLF14
SP9
NRF1
KLF2
SP4
Bits

861

862 **Figure 4. Multiomic analyses of RNA and ATAC modalities of peritoneal macrophages.** (A) Schematic
863 of experimental design. (B) UMAP visualisation based on a weighted combination of RNA and ATAC
864 data from peritoneal macrophages isolated from vehicle treated endometriosis mice, RRx-001 treated
865 endometriosis mice and sham mice. Inset is UMAP projection split by sample ID. (C) Feature plots of
866 *Ptprc* (Cd45), *Itgam* (Cd11b), *Adgre1* (F4/80) and *H2-Ab1* (MHChcII) expression levels. (D) Samples split
867 by cluster composition. (E) Dot plot of featured genes. (F) Chromatin accessibility, gene expression
868 data and peak-gene links for Ccr2 expression in selected macrophage populations. (G) Volcano plot of
869 up- and down-regulated DEGs of pro-resolving LpM compared to pro-disease LpM. (H) Transcription
870 factor footprinting of Cebpb and Gata6 in pro-resolving LpM, pro-disease LpM and prototypical LpM
871 populations. (I) DNA sequence motif enrichment analysis of ATAC data in peritoneal macrophages
872 derived from RRx-001 treated endometriosis mice.

873
874
875
876
877
878
879
880
881
882
883
884
885
886
887
888
889
890
891
892
893
894

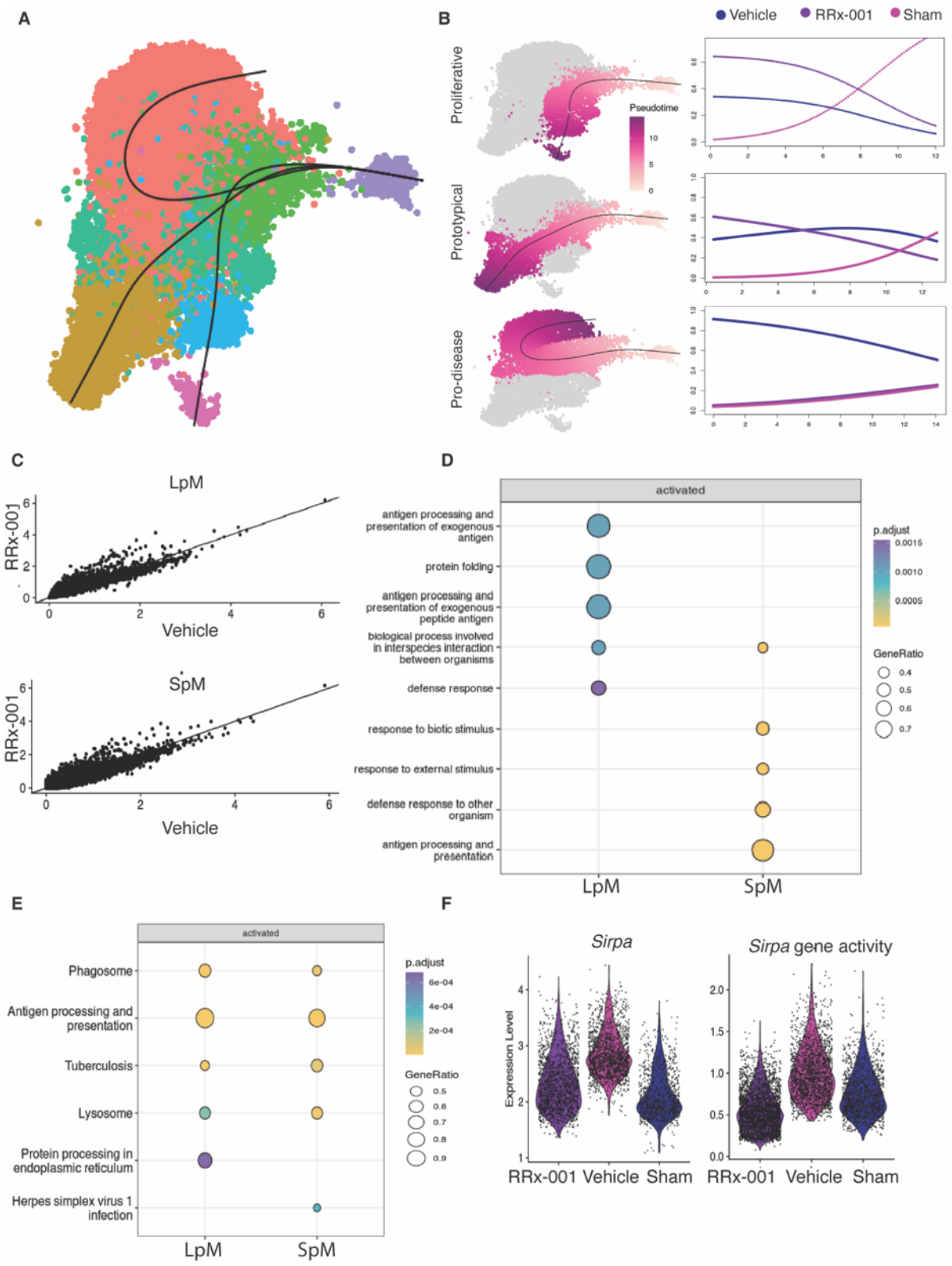

895

896

897 **Figure 5. RRx-001 impacts differentiation trajectories and phenotypes of LpM and SpM populations**
898 **in mice with induced endometriosis.** (A) Slingshot fitted trajectories and principal curves. (B)
899 Pseudotime ordering of inferred lineages (left) with multinomial logistic regression analysis of pseudo-

900 temporal sample imbalance (right). (C) Scatter plot of aggregate (pseudobulk) expression of LpM and
901 SpM populations from RRx-001 and vehicle treated mice (Pearson correlation reported). (D)
902 ClusterProfiler gene set enrichment analysis using GO terms showing the top 5 terms in the LpM and
903 SpM of RRx-001 treated mice with induced endometriosis. (E) ClusterProfiler gene set enrichment
904 analysis using KEGG pathways showing the top 5 pathways in the LpM and SpM of RRx-001 treated
905 mice with induced endometriosis. (F) Violin plots of *Sirp*α expression in RNA-seq data and the gene
906 activity matrix derived from ATAC-seq data.

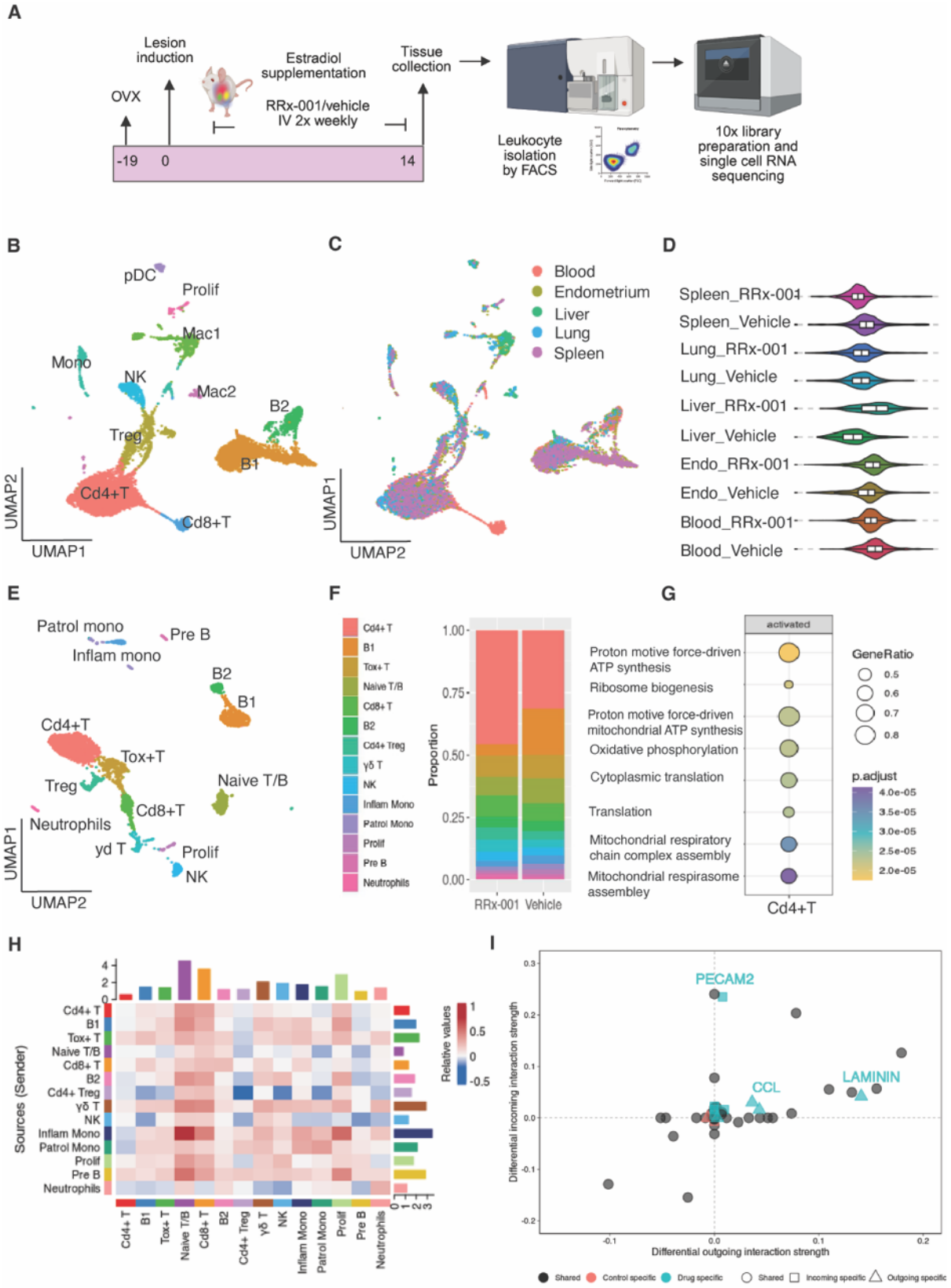

Figure 6. RRx-001 modifies leukocyte immune composition and cell-cell communication in the peripheral blood; distal organs are unaffected (A) Schematic of experimental design. (B) UMAP

visualisation of single cell RNA sequencing data of Cd45+ leukocytes isolated from the peripheral blood, endometrium, liver, lungs and spleen from vehicle and RRx-001 treated endometriosis mice. (C) UMAP split by tissue of origin, (D) violin plot of log10GenesPerUMI from each sample. (E) UMAP visualisation of single cell RNA sequencing data of Cd45+ leukocytes from the peripheral blood only. (F) Peripheral blood samples split by cluster composition. (G) ClusterProfiler gene set enrichment analysis using GO terms showing the top terms activated in the Cd4+ T cells from the peripheral blood of RRx-001 treated mice. (H) CellChat differential interaction strength in the peripheral blood cell-cell communication network between RRx-001 and vehicle treated mice, with red and blue representing increased and decreased signalling, respectively, in RRx-001 treated mice. (I) CellChat signalling changes of inflammatory monocytes in the peripheral blood in RRx-001 and vehicle treated mice.

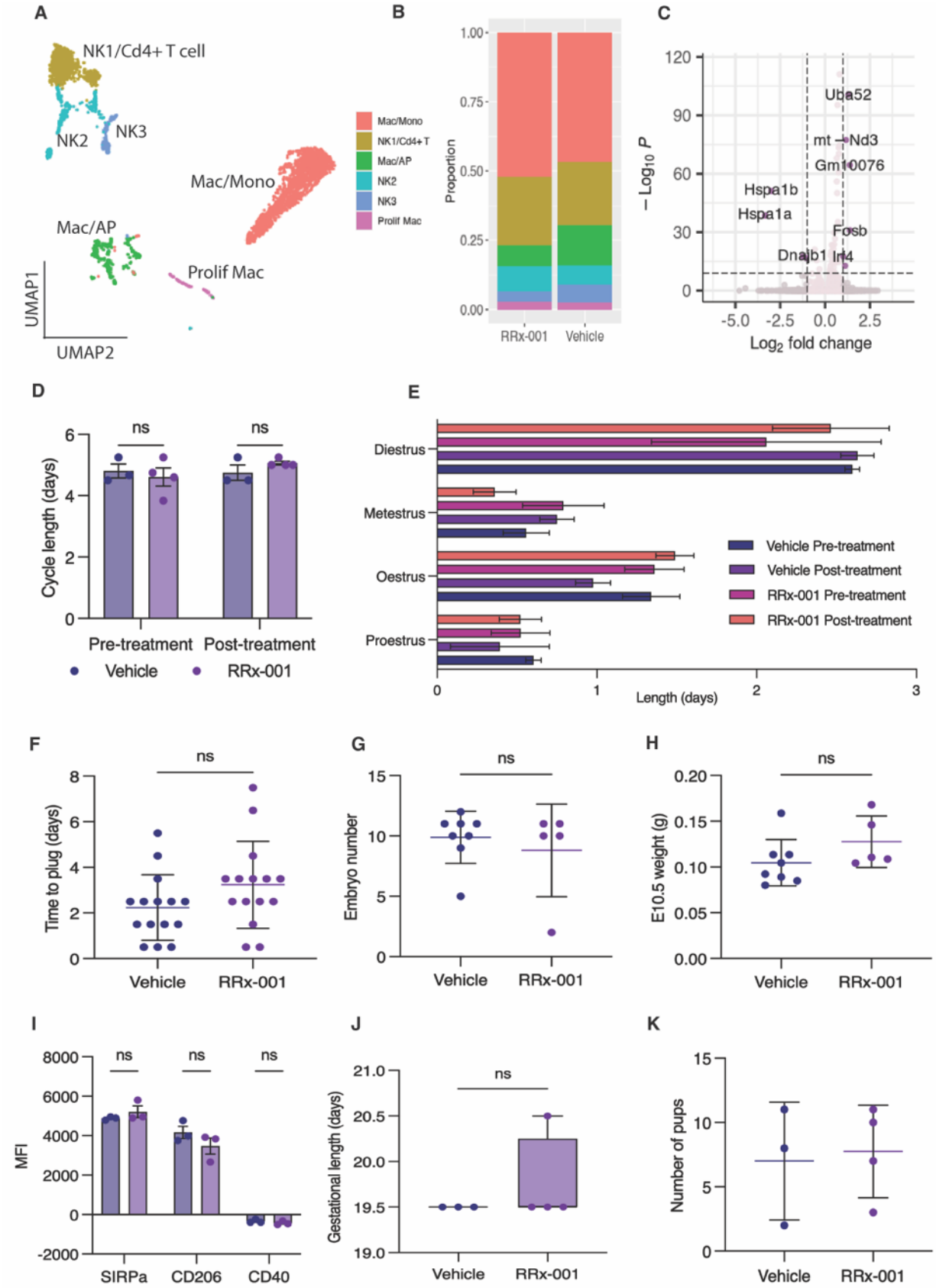
A
NK1/Cd4+ T cell
NK2
NK3
Mac/Mono
Mac/AP
Prolif Mac
UMAP1
UMAP2
Mac/Mono
NK1/Cd4+ T
Mac/AP
NK2
NK3
Prolif Mac
B
Proportion
RRx-001
Vehicle
C
Uba52
mt-Nd3
Gm10076
Hspa1b
Hspa1a
Fosb
Dnajb1
Il4
– Log10 P
Log2 fold change
D
ns
Cycle length (days)
Pre-treatment
Post-treatment
Vehicle
RRx-001
E
Diestrus
Metestrus
Oestrus
Proestrus
Vehicle Pre-treatment
Vehicle Post-treatment
RRx-001 Pre-treatment
RRx-001 Post-treatment
Length (days)
F
Time to plug (days)
G
Embryo number
H
E10.5 weight (g)
I
MFI
SIRPa
CD206
CD40
J
Gestational length (days)
K
Number of pups

948 **Figure 7. Pre-pregnancy treatment with RRx-001 does not modify endometrial macrophages or**
949 **impact reproductive function.** (A) UMAP visualisation of single cell RNA sequencing data of Cd45+
950 leukocytes from the endometrium. (B) Endometrium datasets split by cluster composition. (C)
951 Volcano plot of up and down-regulated DEGs in the Mac/Mono endometrial population between RRx-
952 001 and vehicle treated endometriosis mice. (D) Length of oestrous cycle and (E) days spent within
953 each stage; n=3 vehicle, n=4 RRx-001; statistical analyses performed using Student's t test and two-
954 way ANOVA with Bonferroni post hoc. (F) Time to detection of seminal plug; n=15 RRx-001, n=15
955 vehicle; statistical analysis performed using a Student's t test. (G) Number of embryos and (H) average
956 weight of embryos at E10.5; n=5 RRx-001, n=8 vehicle; statistical analyses performed using a Student's
957 t test. (I) Median fluorescence intensity of SIRPα, CD206 (pro-repair) and CD40 (pro-inflammatory) in
958 Hofbauer cells pooled from 3 placentas per mouse at embryonic day 15.5; n=3 RRx-001, n=4 vehicle,
959 statistical analysis performed using Student's t test. (J) Gestational length of pregnancy and (K)
960 number of pups born to each mouse; n =4 RRx-001, n=3 vehicle. Statistical analyses performed using
961 Student's t tests. No statistical significance reached $p < 0.05$.

962
963
964
965
966
967
968
969
970
971
972
973
974
975
976
977
978
979
980
981

982 **Supplementary Figures**

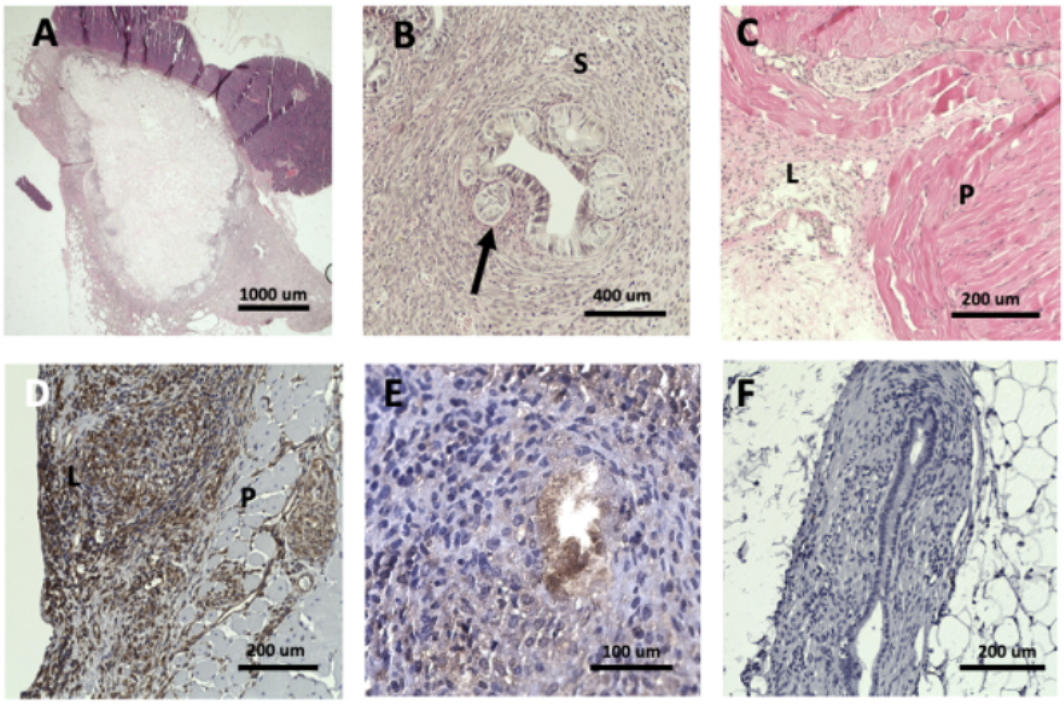

983
984 **Figure S1: Histological verification of lesions.** (A-C) Representative hematoxylin and eosin stains of
985 recovered lesions. (A) Cystic lesion, (B) glandular (arrow) and stromal structures (S) within lesion. (C)
986 Lesion (L) infiltration into the peritoneal wall (P). (D) Stromal (vimentin^{+} cells) on a peritoneal wall
987 lesion. (E) Epithelial (cytokeratin^{+} cells) showing staining of a glandular structure. (F) Negative control.
988 Scale bars as shown.
989
990
991
992
993
994
995
996
997
998
999
1000
1001
1002

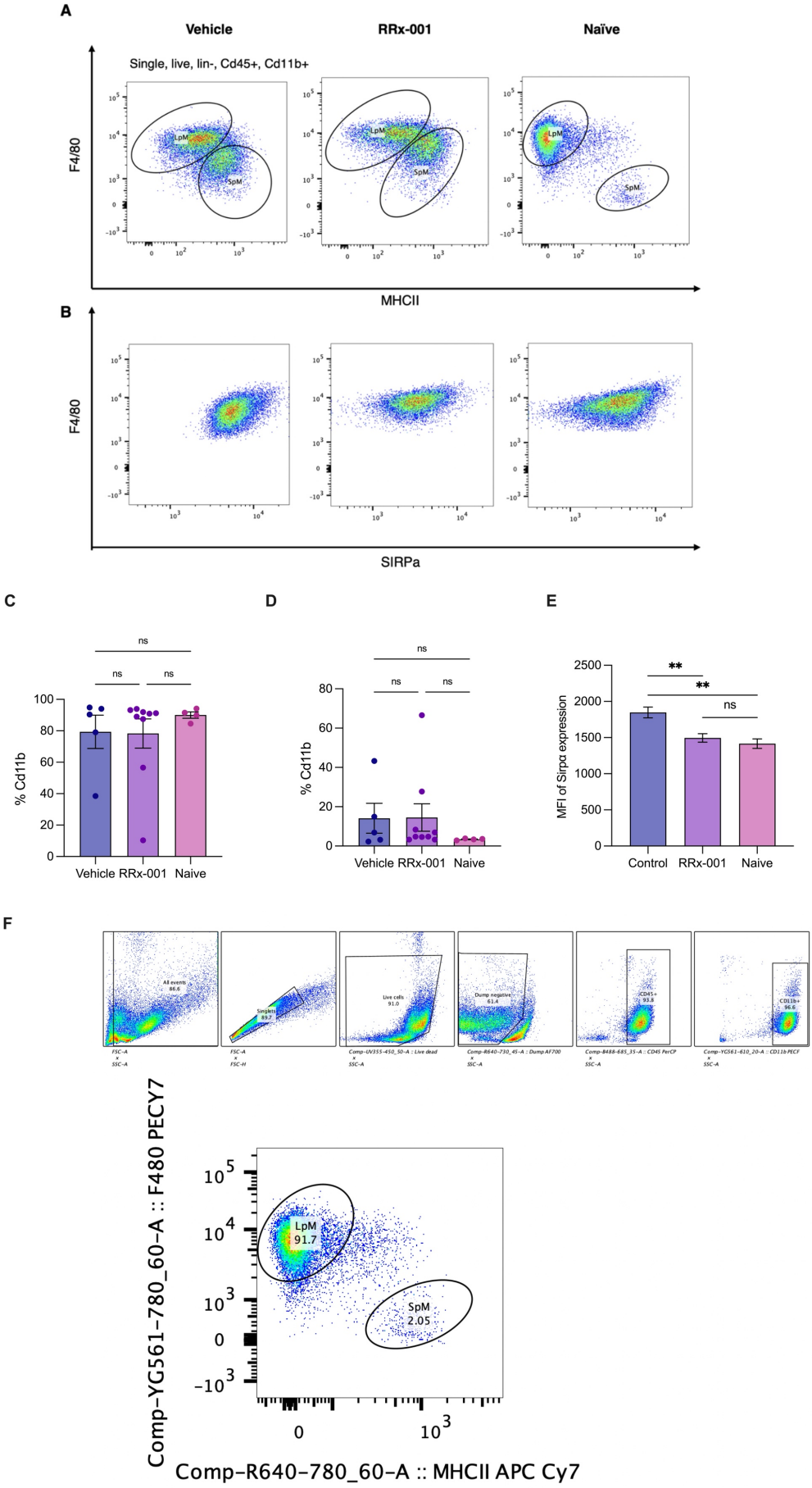
A
Vehicle
RRx-001
Naïve
Single, live, lin-, Cd45+, Cd11b+
F4/80
MHCII
LpM
SpM
B
F4/80
SIRPa
C
% Cd11b
ns
Vehicle RRx-001 Naive
D
% Cd11b
ns
Vehicle RRx-001 Naive
E
MFI of Sirpα expression
**
ns
Control RRx-001 Naive
F
Comp-YG561-780_60-A :: F480 PECY7
Comp-R640-780_60-A :: MHCII APC Cy7
LpM
91.7
SpM
2.05

1003

1004 **Figure S2: Representative flow plots of peritoneal macrophage sub-populations and expression of**
1005 **Sirpα.** (A) Representative flow plots of LpM and SpM populations in vehicle, RRx-001 treated and naïve
1006 mice. (B) LpM population and Sirpα expression. (C) Percentage of Cd11b+ cells that are LpM and (D)
1007 SpM. (E) Median fluorescence intensity of Sirpα on LpM. (F) Flow cytometry gating strategy.
1008
1009

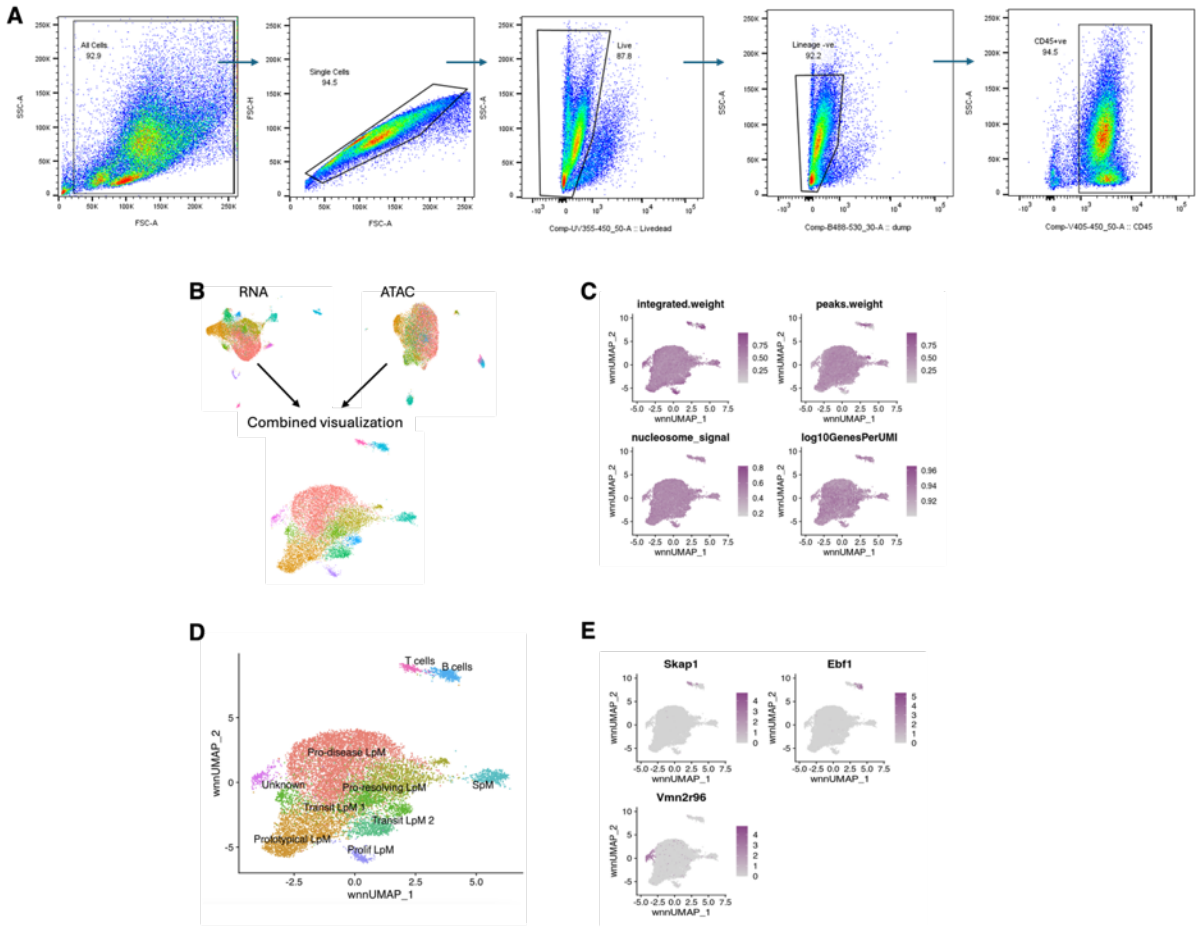

1010
1011 **Figure S3: Isolation of macrophage for integrative weighted nearest neighbours (WNN) analysis.** (A)
1012 Flow cytometry gating strategy. (B) UMAP visualisations of individual RNA and ATAC modalities and
1013 their integrated joint WNN visualisation. (C) RNA and ATAC modality weight across clusters,
1014 nucleosome signal (ATAC) and log10GenesPerUMI (RNA). (D) Clusters corresponding to T, B or
1015 unknown immune cells were removed by identification using marker genes shown in (E) Feature plots
1016 of Skap1, Ebf1 and Vmn2r96, respectively.
1017

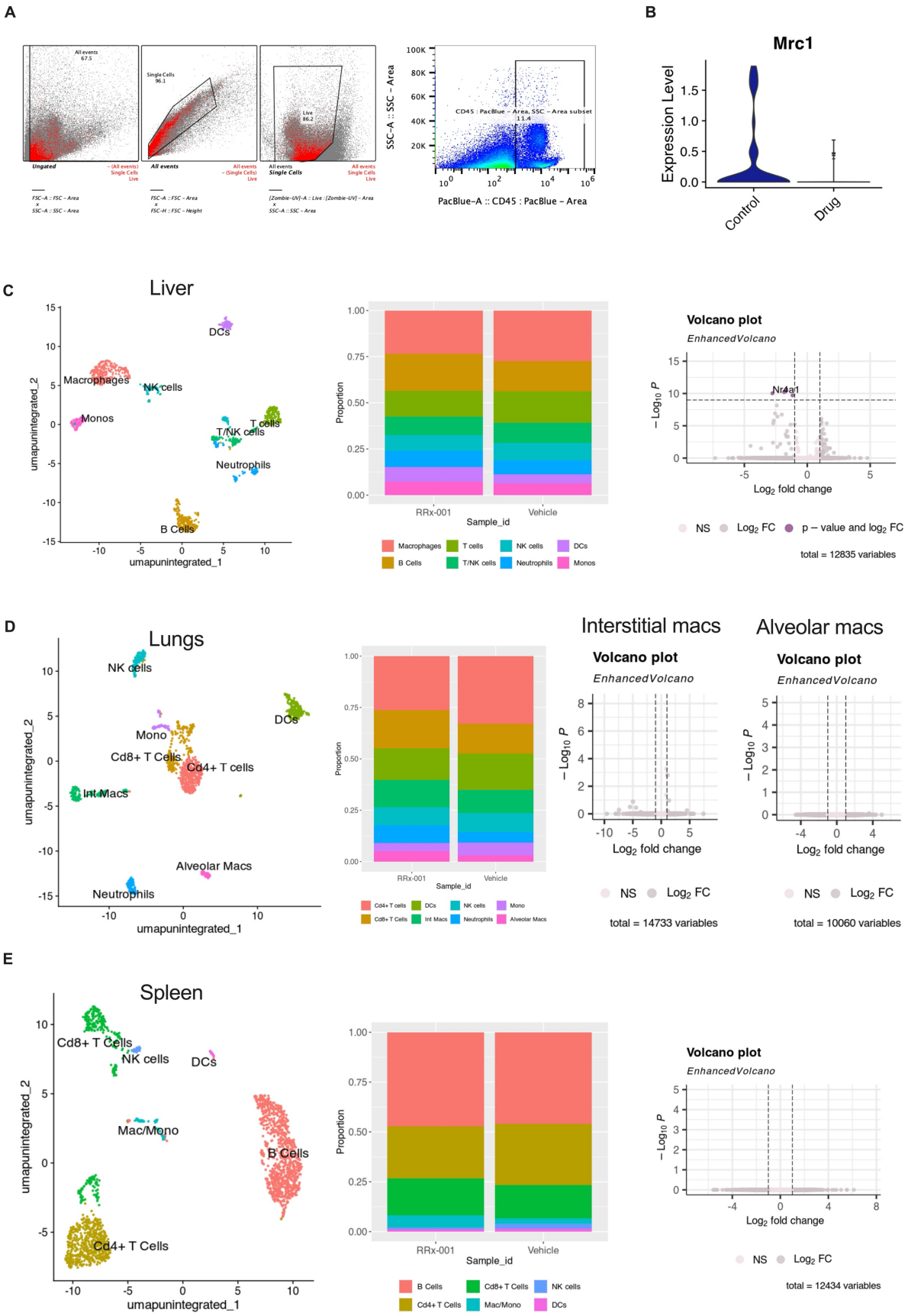

1018

1019

1020

1021 **Figure S4: Gating strategy for isolation of CD45+ leukocytes and the analysis of distal organ immune**
1022 **composition and potential macrophage modification following RRx-001 treatment.** (A) Flow
1023 cytometry gating strategy. (B) Violin plot of Mrc1 on patrolling monocytes. (C) UMAP of Cd45+
1024 leukocytes isolated from the liver of RRx-001 and vehicle treated mice, cluster composition of each
1025 sample, and volcano plot of DEGs between RRx-001 and vehicle treated mice in the macrophage
1026 population. (D) UMAP of Cd45+ leukocytes isolated from the lungs of RRx-001 and vehicle treated
1027 mice, cluster composition of each sample, and volcano plots of DEGs between RRx-001 and vehicle
1028 treated mice in the interstitial and alveolar macrophage populations. (E) UMAP of Cd45+ leukocytes
1029 isolated from the spleen of RRx-001 and vehicle treated mice, cluster composition of each sample, and
1030 volcano plot of DEGs between RRx-001 and vehicle treated mice in the macrophage population.
1031

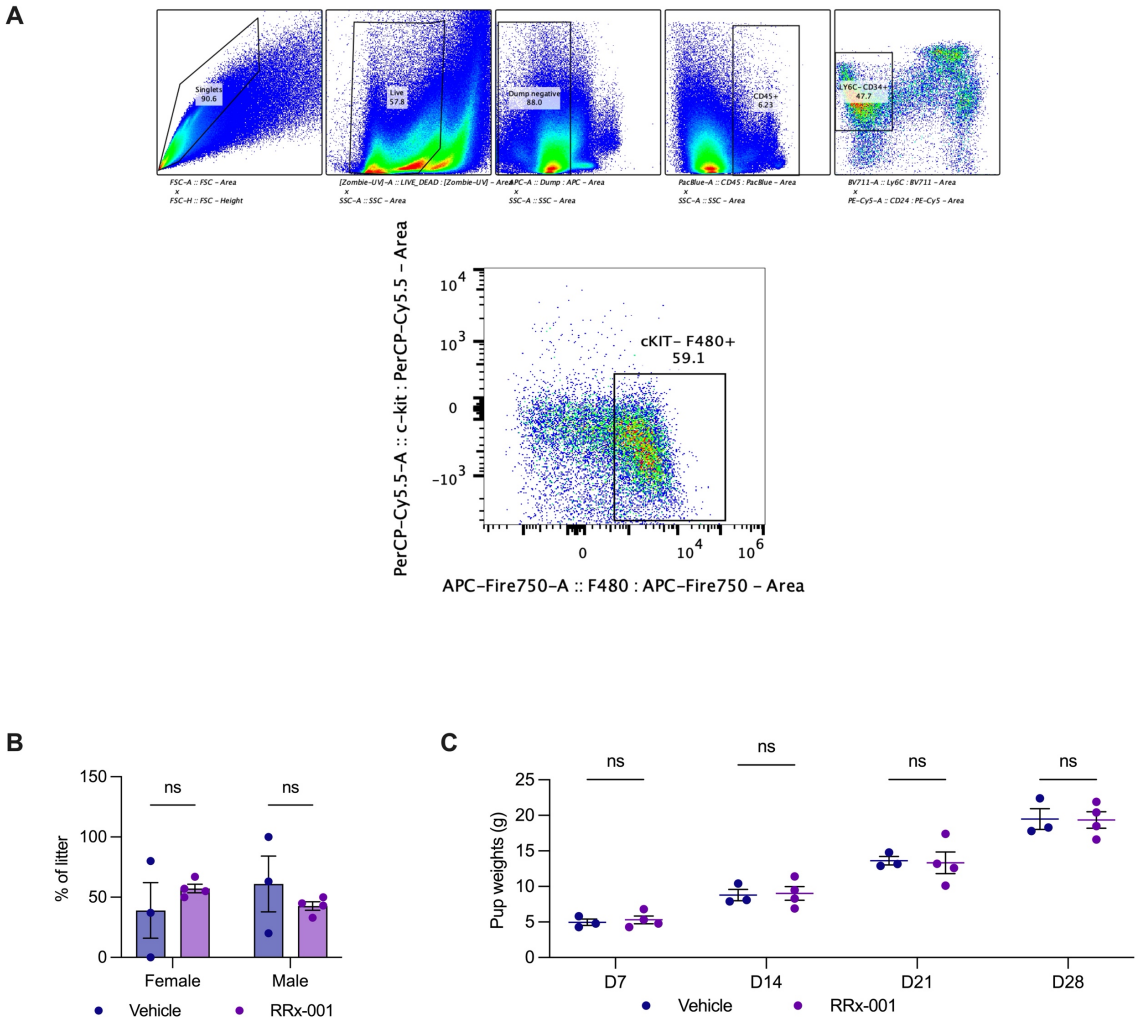

1032
1033 **Figure S5: Gating strategy for isolation of Hofbauer cells and pup reproductive outcomes following**
1034 **pre-pregnancy treatment with RRx-001 or vehicle control.**

(A) Flow cytometry gating strategy. (B) sex ratio of litter and (C) average litter weights from postnatal day 7 to postnatal day 28; n=4 RRx-001, n=3 vehicle. *S*tatistical analyses performed using Student's t tests. No statistical significance reached $p < 0.05$.

References

1. A. L. Shafrir, L. Farland, D. Shah, H. Harris, M. Kvaskoff, K. Zondervan, S. Missmer, Risk for and consequences of endometriosis: a critical epidemiologic review. *Best practice & research Clinical obstetrics & gynaecology* **51**, 1-15 (2018).
2. K. T. Zondervan, C. M. Becker, K. Koga, S. A. Missmer, R. N. Taylor, P. Viganò, Endometriosis. *Nature Reviews Disease Primers* **4**, 9 (2018).
3. T. Hirata, K. Koga, Y. Osuga, Extra-pelvic endometriosis: a review. *Reproductive medicine and biology* **19**, 323-333 (2020).
4. K. T. Zondervan, C. M. Becker, S. A. Missmer, Endometriosis. *N Engl J Med* **382**, 1244-1256 (2020).
5. K. Ellis, D. Munro, J. Clarke, Endometriosis is undervalued: a call to action. *Frontiers in Global Women's Health* **3**, 54 (2022).
6. J. A. Sampson, Metastatic or embolic endometriosis, due to the menstrual dissemination of endometrial tissue into the venous circulation. *The American journal of pathology* **3**, 93 (1927).
7. J. Halme, M. G. Hammond, J. F. Hulka, S. G. Raj, L. M. Talbert, Retrograde menstruation in healthy women and in patients with endometriosis. *Obstetrics and gynecology* **64**, 151-154 (1984).
8. L. K. Symons, J. E. Miller, V. R. Kay, R. M. Marks, K. Liblik, M. Koti, C. Tayade, The immunopathophysiology of endometriosis. *Trends in molecular medicine* **24**, 748-762 (2018).
9. A. W. Horne, S. A. Missmer, Pathophysiology, diagnosis, and management of endometriosis. *bmj* **379**, (2022).
10. R. O. Burney, L. C. Giudice, Pathogenesis and pathophysiology of endometriosis. *Fertility and sterility* **98**, 511-519 (2012).
11. M. H. Wu, K. Y. Hsiao, S. J. Tsai, Hypoxia: The force of endometriosis. *Journal of Obstetrics and Gynaecology Research* **45**, 532-541 (2019).
12. C. Chapron, L. Marcellin, B. Borghese, P. Santulli, Rethinking mechanisms, diagnosis and management of endometriosis. *Nature Reviews Endocrinology* **15**, 666-682 (2019).
13. K. Nirgianakis, L. Ma, B. McKinnon, M. D. Mueller, Recurrence patterns after surgery in patients with different endometriosis subtypes: a long-term hospital-based cohort study. *Journal of clinical medicine* **9**, 496 (2020).
14. G. Dunselman, N. Vermeulen, C. Becker, C. Calhaz-Jorge, T. D'Hooghe, B. De Bie, O. Heikinheimo, A. Horne, L. Kiesel, A. Nap, ESHRE guideline: management of women with endometriosis. *Human reproduction* **29**, 400-412 (2014).
15. C. M. Becker, W. T. Gattrell, K. Gude, S. S. Singh, Reevaluating response and failure of medical treatment of endometriosis: a systematic review. *Fertility and sterility* **108**, 125-136 (2017).
16. C. Hogg, A. W. Horne, E. Greaves, Endometriosis-associated macrophages: origin, phenotype, and function. *Frontiers in endocrinology* **11**, 7 (2020).

1079 17. A. Shapouri-Moghaddam, S. Mohammadian, H. Vazini, M. Taghadosi, S. A. Esmaeili,
1080 F. Mardani, B. Seifi, A. Mohammadi, J. T. Afshari, A. Sahebkar, Macrophage plasticity,
1081 polarization, and function in health and disease. *J Cell Physiol* **233**, 6425-6440 (2018).
1082 18. F. Ginhoux, M. Guilliams, Tissue-resident macrophage ontogeny and homeostasis.
1083 *Immunity* **44**, 439-449 (2016).
1084 19. P. Italiani, D. Boraschi, From monocytes to M1/M2 macrophages: phenotypical vs.
1085 functional differentiation. *Frontiers in immunology* **5**, 514 (2014).
1086 20. M. Bacci, A. Capobianco, A. Monno, L. Cottone, F. Di Puppo, B. Camisa, M. Mariani,
1087 C. Brignole, M. Ponzoni, S. Ferrari, P. Panina-Bordignon, A. A. Manfredi, P. Rovere-Querini,
1088 Macrophages are alternatively activated in patients with endometriosis and required for
1089 growth and vascularization of lesions in a mouse model of disease. *Am J Pathol* **175**, 547-
1090 556 (2009).
1091 21. R. Forster, A. Sarginson, A. Velichkova, C. Hogg, A. Dorning, A. W. Horne, P. T. K.
1092 Saunders, E. Greaves, Macrophage-derived insulin-like growth factor-1 is a key
1093 neurotrophic and nerve-sensitizing factor in pain associated with endometriosis. *Faseb j*
1094 **33**, 11210-11222 (2019).
1095 22. T. N. Ramírez-Pavez, M. Martínez-Esparza, A. J. Ruiz-Alcaraz, P. Marín-Sánchez, F.
1096 Machado-Linde, P. García-Peñarrubia, The role of peritoneal macrophages in
1097 endometriosis. *International Journal of Molecular Sciences* **22**, 10792 (2021).
1098 23. C. C. Bain, C. A. Hawley, H. Garner, C. L. Scott, A. Schridde, N. J. Steers, M. Mack, A.
1099 Joshi, M. Guilliams, A. M. I. Mowat, Long-lived self-renewing bone marrow-derived
1100 macrophages displace embryo-derived cells to inhabit adult serous cavities. *Nature*
1101 *communications* **7**, ncomms11852 (2016).
1102 24. Y. Tan, W. F. Flynn, S. Sivajothi, D. Luo, S. B. Bozal, M. Davé, A. A. Luciano, P. Robson,
1103 D. E. Luciano, E. T. Courtois, Single-cell analysis of endometriosis reveals a coordinated
1104 transcriptional programme driving immunotolerance and angiogenesis across eutopic and
1105 ectopic tissues. *Nat Cell Biol* **24**, 1306-1318 (2022).
1106 25. M. Guo, C. Bafligil, T. Tapmeier, C. Hubbard, S. Manek, C. Shang, F. O. Martinez, N.
1107 Schmidt, M. Obendorf, H. Hess-Stumpp, T. M. Zollner, S. Kennedy, C. M. Becker, K. T.
1108 Zondervan, A. P. Cribbs, U. Oppermann, Mass cytometry analysis reveals a distinct
1109 immune environment in peritoneal fluid in endometriosis: a characterisation study. *BMC*
1110 *Med* **18**, 3 (2020).
1111 26. Y. Henlon, K. Panir, I. McIntyre, C. Hogg, P. Dhami, A. O. Cuff, A. Senior, N.
1112 Moolchandani-Adwani, E. T. Courtois, A. W. Horne, M. Rosser, S. Ott, E. Greaves, Single-
1113 cell analysis identifies distinct macrophage phenotypes associated with pro-disease and
1114 pro-resolving functions in the endometriotic niche. *bioRxiv*, 2024.2003.2007.583861
1115 (2024).
1116 27. G. Zou, J. Wang, X. Xu, P. Xu, L. Zhu, Q. Yu, Y. Peng, X. Guo, T. Li, X. Zhang, Cell
1117 subtypes and immune dysfunction in peritoneal fluid of endometriosis revealed by single-
1118 cell RNA-sequencing. *Cell Biosci* **11**, 98 (2021).
1119 28. J. Li, S. Yan, Q. Li, Y. Huang, M. Ji, X. Jiao, M. Yuan, G. Wang, Macrophage-associated
1120 immune checkpoint CD47 blocking ameliorates endometriosis. *Mol Hum Reprod* **28**,
1121 (2022).
1122 29. C. Hogg, K. Panir, P. Dhami, M. Rosser, M. Mack, D. Soong, J. W. Pollard, S. J. Jenkins,
1123 A. W. Horne, E. Greaves, Macrophages inhibit and enhance endometriosis depending on
1124 their origin. *Proc Natl Acad Sci U S A* **118**, (2021).

30. J. Vallvé-Juanico, A. F. George, S. Sen, R. Thomas, M.-G. Shin, D. Kushnoor, J. J. Vásquez, K. C. Vo, J. C. Irwin, N. R. Roan, Deep immunophenotyping reveals endometriosis is marked by dysregulation of the mononuclear phagocytic system in endometrium and peripheral blood. *BMC medicine* **20**, 1-19 (2022).
31. A. Labani-Motlagh, M. Ashja-Mahdavi, A. Loskog, The tumor microenvironment: a milieu hindering and obstructing antitumor immune responses. *Frontiers in immunology* **11**, 940 (2020).
32. K. Movahedi, D. Laoui, C. Gysemans, M. Baeten, G. Stangé, J. Van den Bossche, M. Mack, D. Pipeleers, P. In't Veld, P. De Baetselier, Different tumor microenvironments contain functionally distinct subsets of macrophages derived from Ly6C (high) monocytes. *Cancer research* **70**, 5728-5739 (2010).
33. E. Azizi, A. J. Carr, G. Plitas, A. E. Cornish, C. Konopacki, S. Prabhakaran, J. Nainys, K. Wu, V. Kiseliovas, M. Setty, Single-cell map of diverse immune phenotypes in the breast tumor microenvironment. *Cell* **174**, 1293-1308. e1236 (2018).
34. Y. Pan, Y. Yu, X. Wang, T. Zhang, Tumor-associated macrophages in tumor immunity. *Frontiers in immunology* **11**, 583084 (2020).
35. A. Mantovani, F. Marchesi, A. Malesci, L. Laghi, P. Allavena, Tumour-associated macrophages as treatment targets in oncology. *Nature reviews Clinical oncology* **14**, 399-416 (2017).
36. A. Mantovani, P. Allavena, F. Marchesi, C. Garlanda, Macrophages as tools and targets in cancer therapy. *Nature Reviews Drug Discovery* **21**, 799-820 (2022).
37. N. Jayabalan, B. Oronsky, P. Cabrales, T. Reid, S. Caroen, A. M. Johnson, N. A. Birch, J. D. O'Sullivan, R. Gordon, A review of RRx-001: a late-stage multi-indication inhibitor of NLRP3 activation and chronic inflammation. *Drugs* **83**, 389-402 (2023).
38. A. Dorning, P. Dhami, K. Panir, C. Hogg, E. Park, G. D. Ferguson, D. Hargrove, J. Karras, A. W. Horne, E. Greaves, Bioluminescent imaging in induced mouse models of endometriosis reveals differences in four model variations. *Dis Model Mech* **14**, (2021).
39. A. Dorning, P. Dhami, K. Panir, C. Hogg, E. Park, G. D. Ferguson, D. Hargrove, J. Karras, A. W. Horne, E. Greaves, Bioluminescent imaging in induced mouse models of endometriosis reveals differences in four model variations. *Disease models & mechanisms* **14**, dmm049070 (2021).
40. B. Oronsky, C. A. Carter, S. Caroen, C. Scribner, A. Oronsky, T. R. Reid, RRx-001, a first-in-class small molecule inhibitor of MYC and a downregulator of CD47, is an" erythrophagoimmunotherapeutic". *OncoImmunology* **9**, 1746172 (2020).
41. K. A. Burns, D. Peterse, C. B. Appleyard, R. Chandler, S.-W. Guo, A. Pearson, E. Persoons, M. S. Anglesio, M. S. Rogers, K. L. Sharpe-Timms, WERF Endometriosis Phenome and Biobanking Harmonisation Project for Experimental Models in Endometriosis Research (EPHect-EM-Homologous): homologous rodent models. *Molecular Human Reproduction* **31**, gaaf021 (2025).
42. K. N. Dodds, V. Fattori, N. A. Andrews, C. B. Appleyard, J. A. Christianson, R. Gomez, S. L. McAllister, S. A. Missmer, J. Nagel, P. Nunez-Badinez, WERF Endometriosis Phenome and Biobanking Harmonisation Project for Experimental Models in Endometriosis Research (EPHect-EM-Pain): methods to assess pain behaviour in rodent models of endometriosis. *Molecular Human Reproduction* **31**, gaaf023 (2025).
43. M. A. Tejada, C. Antunez, P. Nunez-Badinez, B. De Leo, P. T. Saunders, K. Vincent, A. Cano, J. Nagel, R. Gomez, Rodent Animal Models of Endometriosis-Associated Pain:

1171 Unmet Needs and Resources Available for Improving Translational Research in
1172 Endometriosis. *International Journal of Molecular Sciences* **24**, 2422 (2023).
1173 44. Y. Hao, S. Hao, E. Andersen-Nissen, W. M. Mauck, S. Zheng, A. Butler, M. J. Lee, A. J.
1174 Wilk, C. Darby, M. Zager, Integrated analysis of multimodal single-cell data. *Cell* **184**, 3573-
1175 3587. e3529 (2021).
1176 45. L. Zhao, M. Shi, S. Winuthayanon, J. A. MacLean, K. Hayashi, Niclosamide targets the
1177 dynamic progression of macrophages for the resolution of endometriosis in a mouse
1178 model. *Communications Biology* **5**, 1225 (2022).
1179 46. P. A. Louwe, L. Badiola Gomez, H. Webster, G. Perona-Wright, C. C. Bain, S. J. Forbes,
1180 S. J. Jenkins, Recruited macrophages that colonize the post-inflammatory peritoneal niche
1181 convert into functionally divergent resident cells. *Nat Commun* **12**, 1770 (2021).
1182 47. D. Dörr, B. Obermayer, J. M. Weiner, K. Zimmermann, C. Anania, L. K. Wagner, E. M.
1183 Lyras, V. Sapozhnikova, D. Lara-Astiaso, F. Prósper, C/EBPβ regulates lipid metabolism and
1184 Pparg isoform 2 expression in alveolar macrophages. *Science Immunology* **7**, eabj0140
1185 (2022).
1186 48. M. Rosas, L. C. Davies, P. J. Giles, C.-T. Liao, B. Kharfan, T. C. Stone, V. B. O'Donnell, D.
1187 J. Fraser, S. A. Jones, P. R. Taylor, The transcription factor Gata6 links tissue macrophage
1188 phenotype and proliferative renewal. *Science* **344**, 645-648 (2014).
1189 49. Y. Yuan, G. Fan, Y. Liu, L. Liu, T. Zhang, P. Liu, Q. Tu, X. Zhang, S. Luo, L. Yao, F. Chen,
1190 J. Li, The transcription factor KLF14 regulates macrophage glycolysis and immune function
1191 by inhibiting HK2 in sepsis. *Cellular & Molecular Immunology* **19**, 504-515 (2022).
1192 50. B. Oronsky, L. Takahashi, R. Gordon, P. Cabrales, S. Caroen, T. Reid, RRx-001: a
1193 chimeric triple action NLRP3 inhibitor, Nrf2 inducer, and nitric oxide superagonist. *Front*
1194 *Oncol* **13**, 1204143 (2023).
1195 51. M.-J. Lee, Y. Tomita, A. Yuno, S. Lee, N. E. Abrouk, B. Oronsky, S. Caroen, J. B. Trepel,
1196 Results from a biomarker study to accompany a phase II trial of RRx-001 with
1197 reintroduced platinum-based chemotherapy in relapsed small cell carcinoma. *Expert*
1198 *opinion on investigational drugs* **30**, 177-183 (2021).
1199 52. L. Van Putten, F. Croon, The life span of red cells in the rat and the mouse as
1200 determined by labeling with DFP32 in vivo. *Blood* **13**, 789-794 (1958).
1201 53. L. Zhang, W. Long, W. Xu, X. Chen, X. Zhao, B. Wu, Digital cell atlas of mouse uterus:
1202 from regenerative stage to maturational stage. *Frontiers in Genetics* **13**, 847646 (2022).
1203 54. W. K. Whitten, Modification of the oestrous cycle of the mouse by external stimuli
1204 associated with the male. *Journal of Endocrinology* **13**, 399-404 (1956).
1205 55. L. Reyes, B. Wolfe, T. Golos, Hofbauer cells: placental macrophages of fetal origin.
1206 *Macrophages: origin, functions and biointervention*, 45-60 (2017).
1207 56. C. A. Carter, B. Schmitz, P. G. Peterson, M. Quinn, A. Degesys, J. Jenkins, B. Oronsky,
1208 J. Scicinski, S. Caroen, T. R. Reid, Immune reactivity and pseudoprogression or tumor flare
1209 in a serially biopsied neuroendocrine patient treated with the epigenetic agent RRx-001.
1210 *Case reports in oncology* **9**, 164-170 (2016).
1211 57. R. M. Deacon, Assessing nest building in mice. *Nat Protoc* **1**, 1117-1119 (2006).
1212 58. P. Cabrales, RRx-001 acts as a dual small molecule checkpoint inhibitor by
1213 downregulating CD47 on cancer cells and SIRP-α on monocytes/macrophages.
1214 *Translational oncology* **12**, 626-632 (2019).
1215 59. L. Assaf, A. A. Eid, J. Nassif, Role of AMPK/mTOR, mitochondria, and ROS in the
1216 pathogenesis of endometriosis. *Life sciences* **306**, 120805 (2022).

1217 60. X. Yang, X. Xue, Y. Zhu, Z. Zhang, Correlation between lipid metabolism and
1218 endometriosis: a meta-analysis. *Gynecological Endocrinology* **41**, 2500459 (2025).
1219 61. W. Spivia, P. S. Magno, P. Le, D. A. Fraser, Complement protein C1q promotes
1220 macrophage anti-inflammatory M2-like polarization during the clearance of atherogenic
1221 lipoproteins. *Inflammation Research* **63**, 885-893 (2014).
1222 62. S. Pretta, V. Remorgida, L. H. Abbamonte, P. Anserini, N. Ragni, M. Del Sette, C.
1223 Gandolfo, S. Ferrero, Atherosclerosis in women with endometriosis. *European Journal of*
1224 *Obstetrics & Gynecology and Reproductive Biology* **132**, 226-231 (2007).
1225 63. C. Agostinis, M. Toffoli, G. Zito, A. Balduit, S. Pegoraro, M. Spazzapan, L. Pascolo, F.
1226 Romano, G. Di Lorenzo, A. Mangogna, Proangiogenic properties of complement protein
1227 C1q can contribute to endometriosis. *Frontiers in immunology* **15**, 1405597 (2024).
1228 64. H. Zhao, S. Ning, J. Scicinski, B. Oronsky, S. J. Knox, D. M. Peehl, Epigenetic effects of
1229 RRx-001: a possible unifying mechanism of anticancer activity. *Oncotarget* **6**, 43172-43181
1230 (2015).
1231 65. B. Oronsky, X. Guo, X. Wang, P. Cabrales, D. Sher, L. Cannizzo, B. Wardle, N. Abrouk,
1232 M. Lybeck, S. Caroen, Discovery of RRx-001, a Myc and CD47 downregulating small
1233 molecule with tumor targeted cytotoxicity and healthy tissue cytoprotective properties in
1234 clinical development. *Journal of medicinal chemistry* **64**, 7261-7271 (2021).
1235 66. T. Reid, B. Oronsky, J. Scicinski, C. L. Scribner, S. J. Knox, S. Ning, D. M. Peehl, R. Korn,
1236 M. Stirn, C. A. Carter, A. Oronsky, M. J. Taylor, W. L. Fitch, P. Cabrales, M. M. Kim, H. A.
1237 Burris, C. D. Lao, N. E. D. Abrouk, G. R. Fanger, J. R. Infante, Safety and activity of RRx-001
1238 in patients with advanced cancer: a first-in-human, open-label, dose-escalation phase 1
1239 study. *The Lancet Oncology* **16**, 1133-1142 (2015).
1240 67. M. H. Fens, P. Cabrales, J. Scicinski, S. K. Larkin, J. H. Suh, F. A. Kuypers, N. Oronsky,
1241 M. Lybeck, A. Oronsky, B. Oronsky, Targeting tumor hypoxia with the epigenetic
1242 anticancer agent, RRx-001: a superagonist of nitric oxide generation. *Med Oncol* **33**, 85
1243 (2016).
1244 68. B. Oronsky, P. Cabrales, S. Caroen, X. Guo, C. Scribner, A. Oronsky, T. R. Reid, RRx-
1245 001, a downregulator of the CD47- SIRPα checkpoint pathway, does not cause anemia or
1246 thrombocytopenia. *Expert Opin Drug Metab Toxicol* **17**, 355-357 (2021).
1247 69. P. Cabrales, RRx-001 Acts as a Dual Small Molecule Checkpoint Inhibitor by
1248 Downregulating CD47 on Cancer Cells and SIRP-α on Monocytes/Macrophages. *Transl*
1249 *Oncol* **12**, 626-632 (2019).
1250 70. H. Zhao, S. Ning, R. Nolley, J. Scicinski, B. Oronsky, S. J. Knox, D. M. Peehl, The
1251 immunomodulatory anticancer agent, RRx-001, induces an interferon response through
1252 epigenetic induction of viral mimicry. *Clin Epigenetics* **9**, 4 (2017).
1253 71. E. Greaves, F. L. Cousins, A. Murray, A. Esnal-Zufiaurre, A. Fassbender, A. W. Horne,
1254 P. T. Saunders, A novel mouse model of endometriosis mimics human phenotype and
1255 reveals insights into the inflammatory contribution of shed endometrium. *Am J Pathol*
1256 **184**, 1930-1939 (2014).
1257 72. F. L. Cousins, A. Murray, A. Esnal, D. A. Gibson, H. O. Critchley, P. T. Saunders,
1258 Evidence from a mouse model that epithelial cell migration and mesenchymal-epithelial
1259 transition contribute to rapid restoration of uterine tissue integrity during menstruation.
1260 *PLoS One* **9**, e86378 (2014).
1261 73. A. C. McLean, N. Valenzuela, S. Fai, S. A. Bennett, Performing vaginal lavage, crystal
1262 violet staining, and vaginal cytological evaluation for mouse estrous cycle staging
1263 identification. *J Vis Exp*, e4389 (2012).

1264 74. E. Greaves, A. W. Horne, H. Jerina, M. Mikolajczak, L. Hilferty, R. Mitchell, S. M.
1265 Fleetwood-Walker, P. T. Saunders, EP2 receptor antagonism reduces peripheral and
1266 central hyperalgesia in a preclinical mouse model of endometriosis. *Sci Rep* **7**, 44169
1267 (2017).
1268 75. K. Ottersbach, E. Dzierzak, in *Leukemia: Methods and Protocols,* C. W. Eric So, Ed.
1269 (Humana Press, Totowa, NJ, 2009), pp. 335-346.
1270 76. G. Liang, B. Huang, F. Wang, F. Liu, Protocols for isolation and characterization of
1271 mouse placental hemogenic endothelial cells. *STAR protocols* **2**, 100884 (2021).
1272 77. L. Heumos, A. C. Schaar, C. Lance, A. Litinetskaya, F. Drost, L. Zappia, M. D. Lücken, D.
1273 C. Strobl, J. Henao, F. Curion, Best practices for single-cell analysis across modalities.
1274 *Nature Reviews Genetics* **24**, 550-572 (2023).
1275 78. Y. Zhang, T. Liu, C. A. Meyer, J. Eeckhoute, D. S. Johnson, B. E. Bernstein, C.
1276 Nusbaum, R. M. Myers, M. Brown, W. Li, Model-based analysis of ChIP-Seq (MACS).
1277 *Genome biology* **9**, 1-9 (2008).
1278 79. Y. Yoshimura, Y. Muto, N. Ledru, H. Wu, K. Omachi, J. H. Miner, B. D. Humphreys, A
1279 single-cell multiomic analysis of kidney organoid differentiation. *Proceedings of the*
1280 *National Academy of Sciences* **120**, e2219699120 (2023).
1281 80. P.-L. Germain, A. Lun, C. G. Meixide, W. Macnair, M. D. Robinson, Doublet
1282 identification in single-cell sequencing data using scDblFinder. *F1000Research* **10**, (2021).
1283 81. M. D. Young, S. Behjati, SoupX removes ambient RNA contamination from droplet-
1284 based single-cell RNA sequencing data. *Gigascience* **9**, giaa151 (2020).
1285 82. I. Korsunsky, N. Millard, J. Fan, K. Slowikowski, F. Zhang, K. Wei, Y. Baglaenko, M.
1286 Brenner, P.-r. Loh, S. Raychaudhuri, Fast, sensitive and accurate integration of single-cell
1287 data with Harmony. *Nature methods* **16**, 1289-1296 (2019).
1288 83. G. Finak, A. McDavid, M. Yajima, J. Deng, V. Gersuk, A. K. Shalek, C. K. Slichter, H. W.
1289 Miller, M. J. McElrath, M. Prlic, MAST: a flexible statistical framework for assessing
1290 transcriptional changes and characterizing heterogeneity in single-cell RNA sequencing
1291 data. *Genome biology* **16**, 1-13 (2015).
1292 84. T. Stuart, A. Butler, P. Hoffman, C. Hafemeister, E. Papalexi, W. M. Mauck, Y. Hao, M.
1293 Stoeckius, P. Smibert, R. Satija, Comprehensive integration of single-cell data. *cell* **177**,
1294 1888-1902. e1821 (2019).
1295 85. K. Blighe, S. Rana, M. Lewis, EnhancedVolcano: Publication-ready volcano plots with
1296 enhanced colouring and labeling. *R package version* **1**, 10.18129 (2019).
1297 86. T. Stuart, A. Srivastava, S. Madad, C. A. Lareau, R. Satija, Single-cell chromatin state
1298 analysis with Signac. *Nature Methods* **18**, 1333-1341 (2021).
1299 87. G. Yu, L.-G. Wang, Y. Han, Q.-Y. He, clusterProfiler: an R package for comparing
1300 biological themes among gene clusters. *Omics: a journal of integrative biology* **16**, 284-
1301 287 (2012).
1302 88. W. Saelens, R. Cannoodt, H. Todorov, Y. Saeys, A comparison of single-cell trajectory
1303 inference methods. *Nature biotechnology* **37**, 547-554 (2019).
1304 89. K. Street, D. Risso, R. B. Fletcher, D. Das, J. Ngai, N. Yosef, E. Purdom, S. Dudoit,
1305 Slingshot: cell lineage and pseudotime inference for single-cell transcriptomics. *BMC*
1306 *genomics* **19**, 1-16 (2018).
1307 90. E. Blanco-Carmona, Generating publication ready visualizations for Single Cell
1308 transcriptomics using SCpubr. *BioRxiv*, 2022.2002. 2028.482303 (2022).

91. S. Jin, C. F. Guerrero-Juarez, L. Zhang, I. Chang, R. Ramos, C.-H. Kuan, P. Myung, M. V. Plikus, Q. Nie, Inference and analysis of cell-cell communication using CellChat. *Nature communications* **12**, 1088 (2021).